



Cite this article: Bell JB, Aquilina A, Woulds C, Glover AG, Little CTS, Reid WDK, Hepburn LE, Newton J, Mills RA. 2016 Geochemistry, faunal composition and trophic structure in reducing sediments on the southwest South Georgia margin. *R. Soc. open sci.* **3**: 160284. <http://dx.doi.org/10.1098/rsos.160284>

Received: 27 April 2016

Accepted: 25 August 2016

Subject Category:

Earth science

Subject Areas:

ecology/environmental
science/biogeochemistry

Keywords:

methane, Southern Ocean, ecology,
assemblage composition, trophodynamics,
authigenic carbonates

Author for correspondence:

James B. Bell

e-mail: gjybb@leeds.ac.uk

Electronic supplementary material is available at <http://dx.doi.org/10.1098/rsos.160284> or via <http://rsos.royalsocietypublishing.org>.

Geochemistry, faunal composition and trophic structure in reducing sediments on the southwest South Georgia margin

James B. Bell^{1,3}, Alfred Aquilina⁴, Clare Woulds¹,
Adrian G. Glover³, Crispin T. S. Little²,
William D. K. Reid⁵, Laura E. Hepburn⁴,
Jason Newton⁶ and Rachel A. Mills⁴


¹School of Geography and Water@Leeds, and ²School of Earth and Environment, University of Leeds, Leeds LS2 9JT, UK

³Life Sciences, Natural History Museum, Cromwell Road, London SW7 5BD, UK

⁴Ocean and Earth Science, National Oceanography Centre Southampton, University of Southampton, Southampton SO14 3ZH, UK

⁵School of Biology, Newcastle University, Ridley Building, NE1 7RU, UK

⁶NERC Life Sciences Mass Spectrometry Facility, SUERC, East Kilbride G75 0QF, UK

 JBB, 0000-0002-6145-5821; WDKR, 0000-0003-0190-0425

Despite a number of studies in areas of focused methane seepage, the extent of transitional sediments of more diffuse methane seepage, and their influence upon biological communities is poorly understood. We investigated an area of reducing sediments with elevated levels of methane on the South Georgia margin around 250 m depth and report data from a series of geochemical and biological analyses. Here, the geochemical signatures were consistent with weak methane seepage and the role of sub-surface methane consumption was clearly very important, preventing gas emissions into bottom waters. As a result, the contribution of methane-derived carbon to the microbial and metazoan food webs was very limited, although sulfur isotopic signatures indicated a wider range of dietary contributions than was apparent from carbon isotope ratios. Macrofaunal assemblages had high dominance and were indicative of reducing sediments, with many taxa common to other similar environments and no seep-endemic fauna, indicating transitional assemblages. Also similar to other cold seep areas, there were samples of authigenic carbonate, but rather than occurring as pavements or sedimentary

concretions, these carbonates were restricted to patches on the shells of *Axinulus antarcticus* (Bivalvia, Thyasiridae), which is suggestive of microbe–metazoan interactions.

1. Introduction

Cold seeps are discontinuous areas of methane and hydrogen sulfide seepage and are widespread in both shallow and deep water [1,2]. There has been much interest in submarine methane deposits, both for their potential as an energy source but also the threat posed to the climate by the potential release of this potent greenhouse gas [1,3]. Thus, the fate of methane in marine sediments is an area of interest for wider climate science [4–6]. Areas of methane seepage are commonly identifiable by high levels of dissolved methane, bubble plumes/gas flares or bottom simulating reflectors [7–10]. High latitude continental shelf regions are areas with potentially widespread methane storage, particularly in the Arctic and Southern Oceans, where the presence of methane reservoirs has been confirmed or inferred at a number of sites [7,9–17]. Since methane can provide a basis for chemosynthesis, this has clear implications for biogeochemical cycles and the range of available habitats and biodiversity in the polar oceans [18]. Methane-enriched, reducing sediments are part of a continuum between cold seeps and background sediments in the deep sea [19] and may support transitional faunal assemblages. Research into faunal composition and trophic structure in these settings is very limited and here we present for the first time a comprehensive study of geochemical and faunal characteristics of reducing sediments from the Southern Ocean.

Sediments that host an active methane flux to bottom water are often places of elevated biomass and abundance of deep-sea benthos [18,20,21], representing important, localized sources of organic matter for benthic food webs. Such sediments are characterized by elevated methane and hydrogen sulfide concentrations. Sulfide is produced through sulfate reduction during anaerobic oxidation of methane (AOM) [22–25] and can in turn supply reduced chemical species for chemosynthetic reaction pathways that depend upon sulfide oxidation [18,26–28]. Methane-derived carbon (MDC) is an important metabolic resource at high activity seeps [18,21,26,29,30], but the influence of methane-enriched sediments upon trophic structure in areas of lower methane flux is comparatively unknown. MDC is commonly associated with very low $\delta^{13}\text{C}$ signatures (typically -100 to -40‰) compared with other sources of organic matter (typically more than -30‰) [20,30]. AOM can also yield very low $\delta^{34}\text{S}$ signatures as a result of sulfate reduction making stable isotope analysis (SIA) an ideal tool to estimate the extent of MDC utilization [24]. Carbon ($\delta^{13}\text{C} : \delta^{12}\text{C}$) and sulfur ($\delta^{34}\text{S} : \delta^{32}\text{S}$) isotope ratios do not fractionate much between trophic levels and so are useful in detecting differences in food source partitioning. Nitrogen ($\delta^{15}\text{N} : \delta^{14}\text{N}$) isotope ratios provide information on trophic level of individuals or species within a food web as its isotopic signature is increased (approx. 3‰ but can vary widely) during the transfer of proteins from source to consumer [30–32]. Phospholipid fatty acids (PLFAs) can also provide useful insights into the relative abundance and isotopic signatures of certain bacterial biomarkers [33–35]. These compounds degrade quickly following death and so can provide a useful insight into recent microbial activity.

Highly active seeps, typically identified as areas with gas flares or dense aggregations of seep-endemic fauna, have been studied in a number of areas [18,20,21,36,37]. However, the extent, ecology and biogeochemistry of sediments with elevated levels of methane but not sufficiently deep [38] or methane-enriched to support seep-endemic fauna, is not clear. It is possible that, through ocean warming, submarine methane hydrate deposits, which are globally widespread [17,39] will gradually destabilize as bottom temperatures increase, further increasing the extent of such environments [40]. This investigation of the geochemical and biological processes in methane-enriched sediments provides a basis for estimating possible future ecological scenarios.

2. Aims and hypotheses

Around the sub-Antarctic island of South Georgia (54°S), numerous cold seep sites have been identified in fjords along the northern margin [10] (figure 1). We present a combined geochemical and faunal study of reducing sediments on the southwest South Georgia margin, surveyed during two separate expeditions in 2010 and 2011 [15,16] in order to investigate the role of reducing conditions in marine sediment and its impact upon faunal communities with a view to addressing the following hypotheses: (1) faunal community composition is controlled by the extent of reducing conditions, (2) MDC is a

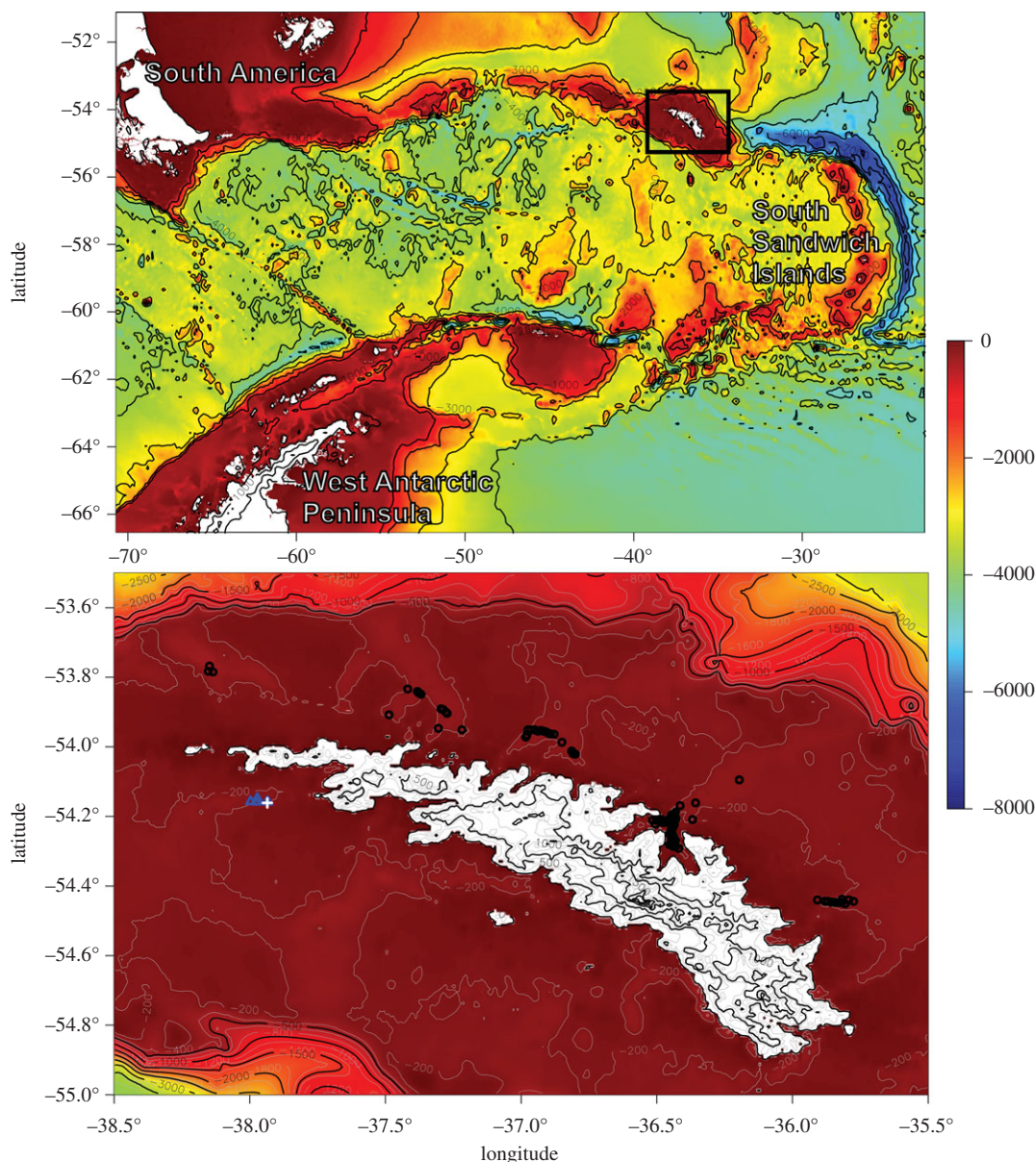


Figure 1. Map of sampling locations around South Georgia. Blue triangles indicate JC42 and JC55 sampling stations. Black circles indicate positions of gas flares [10] and the white cross shows the location of recovered ikaite crystals [41]. Bathymetry data from GEBCO.

significant basal component of the food web and (3) sediments on the South Georgia margin show geochemical signatures consistent with methane seepage.

3. Material and methods

3.1. Sampling

An area of potential methane seepage was originally identified on the southwest South Georgia margin [41]. During a routine fisheries survey, friable samples of what were initially identified as methane hydrate were recovered from a trawl of sulfidic sediments at around 250 m depth (figure 1; [41]). Upon closer inspection, and cross-referencing with environmental conditions, it became apparent that these samples were not methane hydrate but were in fact the metastable authigenic carbonate ikaite (Belchier & Larter 2016, personal communications (figure 2)). The presence of authigenic carbonates, such as ikaite, is sometimes associated with methane seepage [2,42,43], and the area was identified as a site of interest for the study of Southern Ocean marine chemosynthetic ecosystems, though unfortunately the ikaite crystals



Figure 2. Images of seafloor of survey region from towed video platform and crystals of Ikaite recovered [41]. Crystal image courtesy of Mark Belchier. Red laser dots 10 cm apart.

Table 1. Positions (degrees and decimal minutes), depths and usage of JC42 gravity core and JC55 megacore deployments on the southwest South Georgia margin. Three to four cores pooled per deployment for quantitative macrofauna. XRD, X-ray diffraction; SIA, stable isotope analysis; PLFA, phospholipid fatty acids.

cruise	station	sub-station	latitude	longitude	depth (m)	faunal	
						preservation	use(s)
JC42	02_03	1	−54.1575	−37.9761	257	n.a.	Geochemistry
JC55	111	1	−54.1575	−37.9761	257	n.a.	Dissolved O ₂ , PLFAs
	112	1	−54.1575	−37.9761	257	6% Form.	Quant. Macrofauna, Geochemistry, XRD
	113	2	−54.1580	−37.9345	247	80% Etoh	Macrofaunal SIA, Geochemistry, XRD
	117	3	−54.1475	−37.9717	254	6% Form.	Quant. Macrofauna, Geochemistry, Dissolved O ₂
	118	2	−54.1580	−37.9344	247	6% Form.	Quant. Macrofauna, XRD
	119	2	−54.1580	−37.9344	248	80% Etoh	Macrofaunal SIA
	120	2	−54.1580	−37.9344	248	6% Form.	Quant. Macrofauna, XRD
	121	2	−54.1580	−37.9344	248	6% Form.	Quant. Macrofauna
	122	2	−54.1580	−37.9344	248	80% Etoh	Macrofaunal SIA, XRD

quickly degraded after recovery and could not be preserved. During the ‘Chemosynthetic Ecosystems South of the Polar Front’ research programme, the area was visited during two separate expeditions: RRS *James Cook* 42 (JC42, Jan–Feb 2010) and 55 (JC55, Jan–Feb 2011). We report data from sediment geochemistry samples, taken during JC42 and JC55 [15,16], and faunal samples taken during JC55 [16]. We visited three stations on the southwest South Georgia margin (table 1; figure 1) at around 250 m depth, distributed over an area of approximately 7 km².

3.2. Fauna

Fauna were all sampled during JC55 using a Bowers–Connelly dampened megacorer fitted with eight 10 cm diameter tubes [44]. Between one and six deployments were taken from each site (table 1) giving a total area quantitatively sampled of approximately 1490 cm². Between three and four individual cores were pooled from each corer deployment, as cores from the same deployment are pseudoreplicates

[45]. Material retained on a 300 μm sieve was either preserved directly in 10% formalin (in buffered seawater) for quantitative community analyses or live sorted and subsequently preserved in 80% ethanol for on-board photographic documentation and SIA. All faunal samples were sorted under a dissecting microscope to either species/morphospecies level (annelid and bivalve taxa) or higher levels for low abundance taxa (e.g. family level for peracarid crustaceans). Species identities were cross-referenced with the Ocean Biogeographic Information System (OBIS).

3.3. Stable isotopes

A combination of dual- ($\delta^{13}\text{C}$ and $\delta^{15}\text{N}$, 91 samples) and tri- ($\delta^{13}\text{C}$, $\delta^{15}\text{N}$ and $\delta^{34}\text{S}$, 35 samples) isotope techniques was used to describe isotopic signatures of 29 species/morphospecies of macrofauna, sediment organic matter content and profiles of sediment organic carbon. The number of faunal samples submitted for C/N and C/N/S analyses were representative of 88 and 92% of the total faunal abundance, respectively, including the 12 most abundant taxa (1–10 replicates per taxa depending upon abundance/availability of sample mass). Specimens submitted for isotope analyses were pooled if necessary to achieve a specified optimal mass (C/N = 0.7 mg \pm 0.5, C/N/S = 2.5 mg \pm 0.5). Where possible, individual specimens were submitted as separate samples in order to preserve variance structure within populations [46,47] but in some cases, low sample mass meant individuals had to be pooled (e.g. oligochaetes). Specimens were dried for a minimum of 24 hours at 50°C and weighed in mg (correct to 3 d.p.) into ultra-clean tin capsules and stored in a desiccator whilst awaiting SIA.

Subsamples of sediment were taken from two cores (112 and 117; table 1) for organic carbon profiles and freeze-dried. Sediment samples (approx. 1 mg) were acidified using 6 M HCl to remove inorganic carbon. Thus, $\delta^{13}\text{C}$ analyses were acquired from sediment organic carbon (with the carbon content used to calculate percentage organic carbon). Surface samples of freeze-dried sediment from each site (0–1 cm below seafloor (cmbsf)) were also analysed for C/N/S isotopes (untreated for N/S and acidified with 6 M HCl for C) [40].

Only specimens preserved in ethanol were used for SIA in an attempt to regulate the influence of preservation effects. As a result, only faunal specimens from the southeast of the study area could be analysed for isotopic signatures (table 1). Specimens had any attached sediment removed prior to SIA and specimens with carbonate structures (i.e. bivalves) were physically removed from their shells. However, given the low sample mass available and the deleterious effects of acid upon nitrogen and sulfur ratios [48], these could not feasibly be acidified. The vast majority of the species that occurred in sufficient abundance for SIA were annelid taxa with no carbonate structures. A pilot study confirmed that acidification had little impact upon $\delta^{13}\text{C}$ measurements, and it was considered more appropriate to preserve the integrity of nitrogen and sulfur isotope signatures [48,49] at the expense of a small increase in error for carbon isotope measurements. There are usually substantial differences in signatures of methanotrophic and photosynthetic C-fixation pathways, making mixed diets clearly detectable even with an additional $\delta^{13}\text{C}$ error. $\delta^{34}\text{S}$ measurements were also available to aid interpretation of diet.

All bulk elemental analyses were completed at the East Kilbride Node of the Natural Environment Research Council Life Sciences Mass Spectrometry Facility in 2015. Samples were analysed by continuous flow isotope ratio mass spectrometer using a Vario-Pyro Cube elemental analyser (Elementar), coupled with a Delta Plus XP isotope ratio mass spectrometer (Thermo Electron). Each of the runs of C/N and C/N/S isotope analyses used laboratory standards (gelatine and two amino acid–gelatine mixtures) as well as the international standard USGS40 (glutamic acid). C/N/S measurements used the internal standards (MSAG2: (methanesulfonamide/gelatine and methionine) and the international silver sulfide standards IAEA-S1, S2 and S3. All isotope measurements included samples of freeze-dried, powdered *Antimora rostrata* (ANR), an external reference used in other studies of chemosynthetic ecosystems [49,50]. This standard was used to monitor instrumental variation between runs, instruments and studies. Machine error for ANR measurements was 0.09, 0.35 and 0.93 for $\delta^{13}\text{C}$, $\delta^{15}\text{N}$ and $\delta^{34}\text{S}$, respectively. Measurements of ANR were similar to previous studies, excepting $\delta^{15}\text{N}$ from the tri-isotope run, and so these data were discarded. Stable isotope ratios are all reported in delta (δ) per mille (‰) notation, relative to international standards: V-PDB ($\delta^{13}\text{C}$); Air ($\delta^{15}\text{N}$) and V-CDT ($\delta^{34}\text{S}$).

3.4. Phospholipid fatty acids

Phospholipid fatty acid (PLFA) analyses were completed at the James Hutton Institute, University of Aberdeen using 3.38 g of freeze-dried surface (0–1 cm) sediment from megacore deployment 111 (table 1) following the procedure detailed in Main *et al.* [51], which we summarize below. Lipids were extracted

following a method adapted from [52], using a single-phase mixture of chloroform : methanol : citrate buffer (1 : 2 : 0.8 v-v:v). Lipids were fractionated using 6 ml ISOLUTE SI SPE columns, preconditioned with 5 ml chloroform. Freeze-dried extract was taken up in 400 μ l of chloroform, vortex mixed twice and allowed to pass through the column. Columns were washed in chloroform and acetone (eluates discarded) and finally 10 ml of methanol. Methanol eluates were collected in vials, allowed to evaporate under a N₂ atmosphere and frozen at -20°C .

PLFAs were derivitized with methanol to produce fatty acid methyl esters (FAMES). Samples were taken up in 1 ml of 1 : 1 (v : v) mixture of methanol and toluene. Then 1 ml of 0.2 M KOH (in methanol) was added with a known quantity of the C19 internal standard (nonadecanoic acid), vortex mixed and incubated at 37°C for 15 min. After cooling to room temperature, 2 ml of isohexane : chloroform (4 : 1 v:v), 0.3 ml of 1 M acetic acid and 2 ml of deionized water were added to each vial. The solution was mixed and centrifuged and the organic phase transferred to a new vial and the remaining aqueous phase was mixed and centrifuged again to further extract the organic phase, which was combined with the previous. The organic phases were evaporated under a N₂ atmosphere and frozen at -20°C .

Samples were taken up in isohexane to perform gas chromatography–combustion–isotope ratio mass spectrometry (GC-C-IRMS). The quantity and $\delta^{13}\text{C}$ values of individual FAMES were determined using a GC Trace Ultra with combustion column attached via a GC Combustion III to a Delta V Advantage isotope ratio mass spectrometer (Thermo Finnigan, Bremen). The $\delta^{13}\text{C}$ values (‰) of each FAME were calculated with respect to a CO₂ monitoring gas, traceable to IAEA reference material NBS 19 TS-Limestone. Measurement of the Indiana University reference material hexadecanoic acid methyl ester (certified $\delta^{13}\text{C}_{\text{VPDB}} 30.74 \pm 0.01$ ‰) gave a value of 30.91 ± 0.31 ‰ (mean \pm s.d., $n = 51$).

Combined areas of all mass peaks (m/z 44, 45 and 46), following background correction, were collected for each FAME. These areas, relative to the internal C19 standard, were used to quantify abundance of each FAME and related to the PLFAs from which they are derived [53]. Compounds were compared with previous studies to identify biomarkers of specific bacterial processes or groups [34,35,54–61]. Bacterial biomass was calculated using transfer functions from the total mass of four PLFAs (i14:0, i15:0, a15:0 and i16:0), estimated at 14% of total PLFA biomass. PLFA biomass is estimated at 5.6% of total bacterial biomass [33].

3.5. Geochemistry sampling

A gravity core (*ca* 200 cm long) was retrieved during JC42 from a water depth of 257 m (JC42 02_03; table 1). This was divided into 50 cm long sections using a circular saw on board, and a nylon wire was used to split each section in two vertically: one half was used for analysis and the other was archived at -20°C . During JC55, sediment samples were collected using a Bowers & Connelly Megacorer [44] equipped with multiple polycarbonate tubes (10 cm diameter). These sediment cores (18–27 cm in length) were retrieved from three sites at water depths of 247–257 m (table 1). Gravity core sections and sampled megacores were immediately transferred into a glove bag under oxygen-free (N₂ atmosphere) and temperature-controlled conditions (*ca* 4–6 $^{\circ}\text{C}$). Gravity core sections were subsampled with a clean spatula at intervals of 5–10 cm. Sampled megacores were manually extruded (at intervals of 1–2 cm) into a polycarbonate ring and sectioned using a PTFE sheet that was cleaned with de-ionized water between samples. Bottom water temperatures were 1.2 $^{\circ}\text{C}$.

3.6. Geochemistry analysis

Dissolved methane in sediment samples was measured as soon as possible after core collection using the headspace vial method [62]. In brief, open-ended, graduated plastic syringes were used to measure an aliquot (3 ml) of wet sediment, which was then extruded into a 20 ml glass vial, followed by 5.0 ml of 1.0 M NaOH to terminate microbial activity. The vial was crimped shut, shaken vigorously for several minutes and left to stand for more than 1 hour. The headspace was then sampled by syringe and the methane was analysed by GC-FID (Agilent 7890A).

Sediment porosity was calculated from the loss of water after drying the sediment at 60°C assuming densities of 2.6 and 1.025 g cm⁻³ for the sediment and pore fluid, respectively [63].

Shipboard determinations of dissolved oxygen content in the upper sediment were carried out on a dedicated core from two sites (table 1). A Unisense OX50 micro-sensor was calibrated between O₂-saturated and anoxic seawater solutions with temperature and salinity equivalent to bottom waters. Unisense micro-profiling apparatus and SENSORTTRACE PRO software resolved oxygen content at 100

and 200 μm intervals downcore. Oxygen profiles were later surface-normalized to bottom water values determined from water samples taken from deployments near the seafloor to convert to $\mu\text{mol kg}^{-1}$.

Pore water was separated from the sediment matrix by centrifugation at 12 000g at 4°C for 10 min under N_2 ; the supernatant fluids were filtered under N_2 through disposable 0.2 μm cellulose nitrate membrane syringe filters (Whatman, UK). Filtered pore waters were divided for H_2S , total alkalinity (TA), dissolved sulfate and dissolved metals (including Fe and Mn). H_2S , TA and dissolved sulfate were determined onboard and samples for dissolved metal analysis were acidified ($\text{pH} < 2$) by adding 2 μl of concentrated HCl (UpA, Romil) per 1 ml of sample, pending analysis at the National Oceanography Centre, Southampton. Elemental abundances in pore waters were determined by inductively coupled plasma (ICP)-atomic absorption spectroscopy (Perkin Elmer Optima 4300DV). Instrument precision was better than 2% and measurements of an artificial seawater standard (CRM-SW) were within 1% of the recommended values.

TA and H_2S were measured immediately following pore water extraction: TA by titrating against 0.10M HCl while bubbling nitrogen through the sample [64] and H_2S using standard photometric procedures based on formation of methylene blue [65]. Sulfate was measured by ion chromatography (Dionex ICS2500), with reproducibility better than 2% (determined by repeat analysis of a seawater standard).

3.7. X-ray diffractometer analyses

During sorting, it was noted that the valves of *Axinulus antarcticus* (Bivalvia: Thyasiridae; Zelaya, 2010) were often partially coated in deposits of yellow, superficially amorphous material, typically close to the antero-dorsal margin. To determine the composition of these deposits, samples were scraped off the shells of the specimens and analysed using an X-ray diffractometer (XRD). Two samples of these deposits were submitted, as well as one of freeze-dried sediment as a control (table 1). Owing to an instrument failure, the first shell deposit sample was analysed using a different instrument to the second shell deposit sample and sediment sample. The first shell deposit sample was analysed using a Bruker D8 diffractometer and a Lynxeye detector. The remaining samples were analysed using a Philips PW1050 diffractometer and a point detector. Both systems used a $\theta / -2\theta$ goniometer and Cu K α -1 radiation.

3.8. Statistical analyses

The following analyses were conducted in the R environment [66], using the Vegan library (v. 2.0–8) [67] unless otherwise specified. Only quantitatively preserved cores were used in assemblage composition analyses. Abundance data from quantitative cores was standardized to individuals per square metre. Community composition from these sites were compared to the composition of Antarctic shelf sediments and cold seep sites in the Pacific [68–70] using the metaMDS and PERMANOVA routine (999 permutations) [71]. Estimated species richness (100 individuals, 999 permutations) was calculated in EstimateS (v. 9.1.0) [72].

4. Results

4.1. Faunal community composition

A total of 4413 animal specimens were counted. Polychaetes dominated all samples (49–70%) with oligochaetes (15–34%) and bivalves (10–12%) accounting for most of the remaining taxa. The most abundant species was *Aphelochaeta glandaria* (Polychaeta: Cirratulidae; Blake, 1996) (1556 ind. counted, up to 14 420 ind. m^{-2}), but also occurring in significant abundances were *Tubificoides* sp. (Oligochaeta: Tubificidae; Lastoĉkin, 1937) (500 ind. counted, up to 8531 ind. m^{-2}), *Psamathe fauveli* (Polychaeta: Hesionidae; Averincev, 1962) (664 ind. counted, up to 5178 ind. m^{-2}) and *Axinulus antarcticus* (Bivalvia) (456 ind. counted, up to 3756 ind. m^{-2}) (table 2). Many specimens of *A. antarcticus* had an unidentified hydrozoan attached to the dorsal margin. These hydrozoan specimens fragmented and detached from their hosts and as such their abundance could not be quantified.

Alpha diversity and estimated species richness were qualitatively similar in all deployments (table 3). Sub-station 1 had the greatest proportion of oligochaetes (34%, compared with 15–22% elsewhere) and the lowest proportion of polychaetes (49%, compared with 64–70% elsewhere). No significant differences were observed in the composition between each of the sub-stations (PERMANOVA, $F = 0.79$, $p = 0.795$).

Table 2. Macrofaunal assemblage composition (quantitative cores only, abundance per m²) and stable isotopic data. A = 0–5 cmbsf, B = 5–10 cmbsf.

taxa			core				
class	genus/other	species	112	117	118	120	121
Polychaeta	<i>Parougia</i>	spA	95.50	466.87	318.32	31.83	445.64
	<i>Scoletoma</i>	<i>tetraura</i>	286.49	721.52	190.99	413.81	477.48
	Aphroditidae	Aphroditidae sp.	95.50	0.00	0.00	0.00	0.00
	Polynoidae	Polynoidae sp.	0.00	0.00	0.00	31.83	0.00
	Sigalionidae	Sigalionidae sp.	0.00	0.00	31.83	0.00	0.00
	Chrysopetalidae	Chrysopetalidae sp.	0.00	127.33	127.33	31.83	31.83
	<i>Psamathe</i>	<i>fauveli</i>	1305.10	5177.96	3215.01	2864.86	4169.96
	<i>Exogone</i>	(<i>parexogone</i>) <i>tasmanica</i>	509.31	594.19	477.48	286.49	445.64
	<i>Sphaerosyllis</i>	<i>hirsuta</i>	572.97	1485.48	732.13	700.30	954.95
	Syllides	sp.	286.49	212.21	127.33	63.66	95.50
	<i>Aglaophamus</i>	<i>trissophyllus</i>	0.00	84.88	0.00	0.00	0.00
	<i>Sphaerodoropsis</i>	<i>parva</i>	541.14	933.73	381.98	254.65	509.31
	<i>Sphaerodoropsis</i>	<i>arctowskyensis</i>	63.66	0.00	0.00	0.00	0.00
	Sphaerodorum	spA	31.83	42.44	0.00	0.00	63.66
	Phyllodocidae	Phyllodocidae sp.	0.00	42.44	0.00	0.00	0.00
	Apistobrachidae	Apistobrachidae sp.	31.83	42.44	63.66	31.83	31.83
	<i>Laonice</i>	<i>wedellia</i>	0.00	0.00	0.00	63.66	31.83
	<i>Spiophanes</i>	<i>croeyeri</i>	222.82	42.44	350.15	159.16	127.33
	Spionidae	Spionidae sp.	0.00	0.00	31.83	0.00	0.00
	<i>Aphelochaeta</i>	<i>glandaria</i>	5634.22	10 483.26	14 419.78	10 122.50	11 491.26
	<i>Aphelochaeta</i>	<i>monilaris</i>	1209.61	169.77	318.32	1145.94	604.80
	<i>Tharyx</i>	<i>marioni</i>	0.00	169.77	0.00	63.66	254.65
	<i>Aphelochaeta</i>	sp. indet/juveniles	0.00	0.00	445.64	572.97	222.82
	<i>Diplocirrus</i>	<i>becci</i> sp. nov	413.81	551.75	63.66	31.83	159.16
	Sternaspidae	Sternaspidae sp.	0.00	169.77	0.00	0.00	31.83
	Ampharetidae	sp. indet	31.83	0.00	0.00	0.00	0.00
	<i>Glyphantostomum</i>	sp.	31.83	42.44	0.00	0.00	0.00
	Polycirrus	sp. indet/juveniles	31.83	0.00	31.83	0.00	0.00
	<i>Hauchiella</i>	<i>tribullata</i>	63.66	42.44	159.16	63.66	254.65
	Polycirrus	sp.	0.00	42.44	0.00	0.00	0.00
	Terebellidae	sp.	31.83	0.00	0.00	0.00	0.00
	Trichobrachidae	Trichobrachidae sp.	222.82	84.88	0.00	31.83	0.00
	<i>Capitella</i>	spA	0.00	0.00	0.00	159.16	0.00
	<i>Capitella</i>	spB	0.00	0.00	0.00	0.00	31.83
	<i>Maldane</i>	<i>sarsi antarctica</i>	31.83	0.00	63.66	0.00	63.66
	<i>Clymenella</i>	<i>antarctica</i>	31.83	42.44	63.66	0.00	0.00
	Opheliidae	Opheliidae sp.	0.00	0.00	95.50	31.83	31.83
	<i>Leitoscoloplos</i>	<i>kerquelensis</i>	0.00	84.88	31.83	0.00	0.00
	<i>Leitoscoloplos</i>	<i>kerquelensis minutus</i>	31.83	0.00	0.00	0.00	0.00

(Continued.)

Table 2. (Continued.)

taxa			core				
class	genus	species	112	117	118	120	121
	<i>Aricidea</i>	<i>antarctica</i>	668.47	679.08	859.46	350.15	1018.62
	<i>Levinsenia</i>	<i>gracilis</i>	31.83	84.88	159.16	0.00	95.50
	<i>Scalibregma</i>	<i>inflatum</i>	0.00	0.00	0.00	95.50	95.50
Bivalvia	<i>Axinulus</i>	<i>antarcticus</i>	2864.86	3225.62	3215.01	2260.05	3756.15
	<i>Propeleda</i>	<i>sp. cf longicaudata</i>	63.66	169.77	0.00	95.50	95.50
	<i>Ennucula</i>	<i>sp.</i>	127.33	127.33	63.66	95.50	445.64
	<i>Mysella</i>	<i>antarctica</i>	63.66	0.00	31.83	0.00	63.66
Clitellata	<i>Limnodriloides</i>	<i>spA</i>	127.33	6069.25	1464.26	2801.19	2482.88
	<i>Tubificoides</i>	<i>spA</i>	8530.91	1612.81	2291.89	2164.56	1718.91
	<i>Limnodriloides</i>	<i>spB</i>	31.83	0.00	31.83	0.00	0.00
Malacostraca	Lysianassidae		0.00	42.44	31.83	0.00	0.00
	Phoxocephalidae		95.50	169.77	413.81	190.99	190.99
	Synopiidae		0.00	127.33	190.99	95.50	254.65
	Ampeliscidae		0.00	0.00	31.83	0.00	0.00
	Sphaeromatidae		0.00	0.00	31.83	0.00	0.00
	Idoteidae		0.00	0.00	63.66	0.00	31.83
	Antarcturidae		0.00	42.44	0.00	31.83	0.00
	Gynodiastylidae		0.00	42.44	63.66	0.00	0.00
	Pseudocumatidae		0.00	42.44	31.83	0.00	63.66
	Lampropridae		0.00	0.00	31.83	0.00	0.00
	Mysida		0.00	84.88	31.83	63.66	31.83
	Tanaidae		0.00	0.00	0.00	0.00	63.66
	Neotanaidae		95.50	127.33	63.66	0.00	0.00
Ophiuroidea	Ophiurina		31.83	42.44	31.83	0.00	0.00
Holothuroidea	Holothuroidea		0.00	0.00	0.00	0.00	31.83
Ascidiacea	Ascidiacea		127.33	84.88	190.99	0.00	0.00
Annelida	Echiura	<i>spB</i>	31.83	0.00	0.00	0.00	31.83
	Sipuncula		700.30	509.31	445.64	190.99	604.80

Table 3. Faunal abundance, diversity and species richness of macrofauna from quantitatively sampled cores. Proportion of individuals counted to total density varied as a result of different numbers of pooled cores between deployments.

JC55 station	sub-station	Ind. counted	Ind. m ⁻²	species observed	diversity (H')	estimated species richness (n = 100) (±s.d.)
112	1	798	25 402	40	2.27	16.81 (2.55)
117	3	828	35 142	43	2.38	17.60 (2.56)
118	2	990	31 513	45	2.18	17.57 (2.43)
120	2	804	25 593	34	2.18	15.85 (2.24)
121	2	993	31 609	41	2.36	18.23 (2.36)

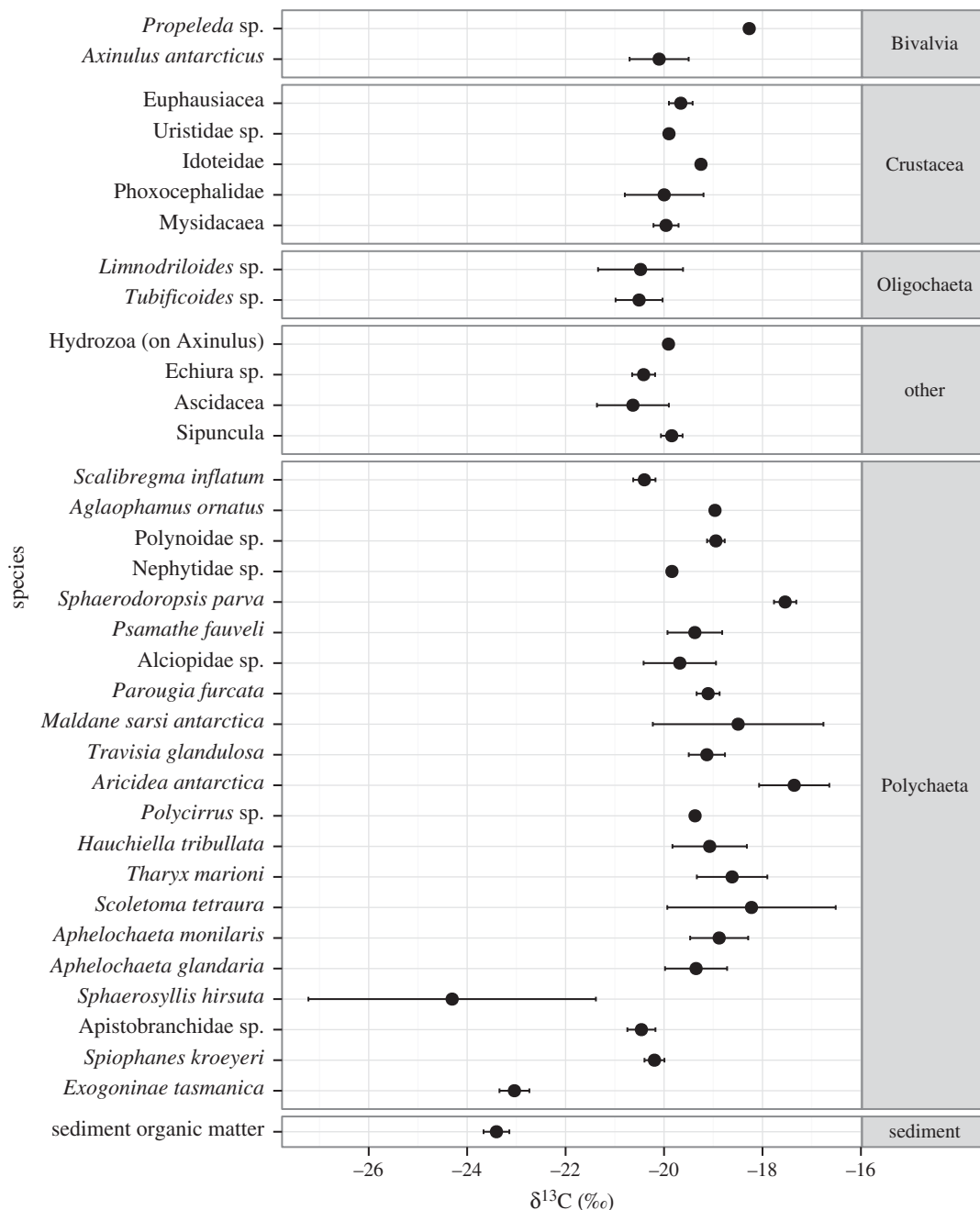


Figure 3. Species and sediment organic matter $\delta^{13}\text{C}$ and $\delta^{15}\text{N} \pm 1$ s.d., grouped by higher taxa.

4.2. Isotopic analyses

Since only ethanol-preserved specimens were used for isotopic measurements, all faunal samples were from the second sub-station (table 1). Measurements of $\delta^{13}\text{C}$ ranged from -26.37 to -15.87‰ across all faunal samples (mean: $-19.55\text{‰} \pm$ s.d. 1.48). $\delta^{15}\text{N}$ values ranged from 4.20 to 12.40‰ (mean: $8.28\text{‰} \pm$ s.d. 1.68; figure 3). Sediment organic material had low $\delta^{15}\text{N}$ values ($5.87\text{‰} \pm 0.91$), indicating that it was the base of the food chain for most species. Several species also had a low $\delta^{15}\text{N}$ signature similar to sediment organic matter (figure 3), suggesting an additional ^{15}N -depleted source of organic nitrogen. All faunal $\delta^{34}\text{S}$ signatures were less than that of surface sediment organic matter (OM) ($14.03 \pm 0.12\text{‰}$) and varied widely ($\delta^{34}\text{S}$ mean: $4.25\text{‰} \pm$ s.d. 5.13, -9.36 – 14.11‰), indicating at least two sources of organic sulfur (figure 4).

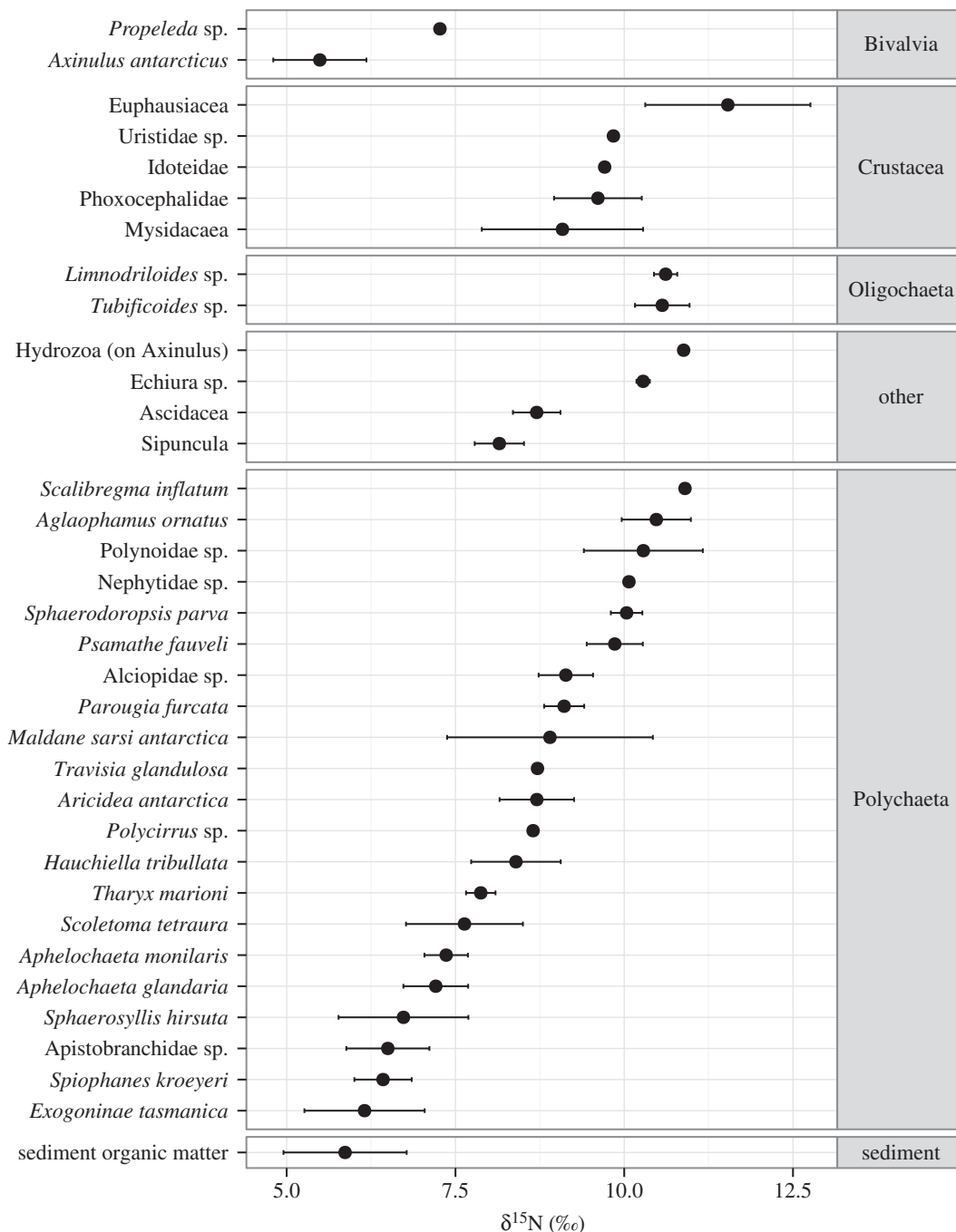


Figure 3. (Continued).

4.3. Poly-unsaturated fatty acids

A total of 34 compounds were identified, ranging in concentration between 0.006 and 1.637 μg per g freeze-dried sediment. These comprise 15 saturated fatty acids, 14 mono-unsaturated fatty acids (MUFAs) and 5 poly-unsaturated fatty acids. Most of the compounds occurred in low abundance (16 < 1% of total, 29 < 5%). The most abundant PLFAs were: C16:0 (1.637 $\mu\text{g g}^{-1}$ sediment, 16.56% of total); C16:1 ω 7c (1.509 $\mu\text{g g}^{-1}$, 15.39%); C18:1 ω (10 or 11) (1.301 $\mu\text{g g}^{-1}$, 13.51%) and C18:1 ω 7 (1.188 $\mu\text{g g}^{-1}$, 12.34%). Carbon isotopic signatures of PLFAs ranged between -45.60 and -23.85 ‰ ($\delta^{13}\text{C}$ mean -31.17 ‰). Bacterial total biomass was estimated from the concentration of i14:0, i15:0, ai15:0 and i16:0 at 113.14 $\mu\text{g g}^{-1}$ sediment (115.97 $\mu\text{g cm}^{-3}$).

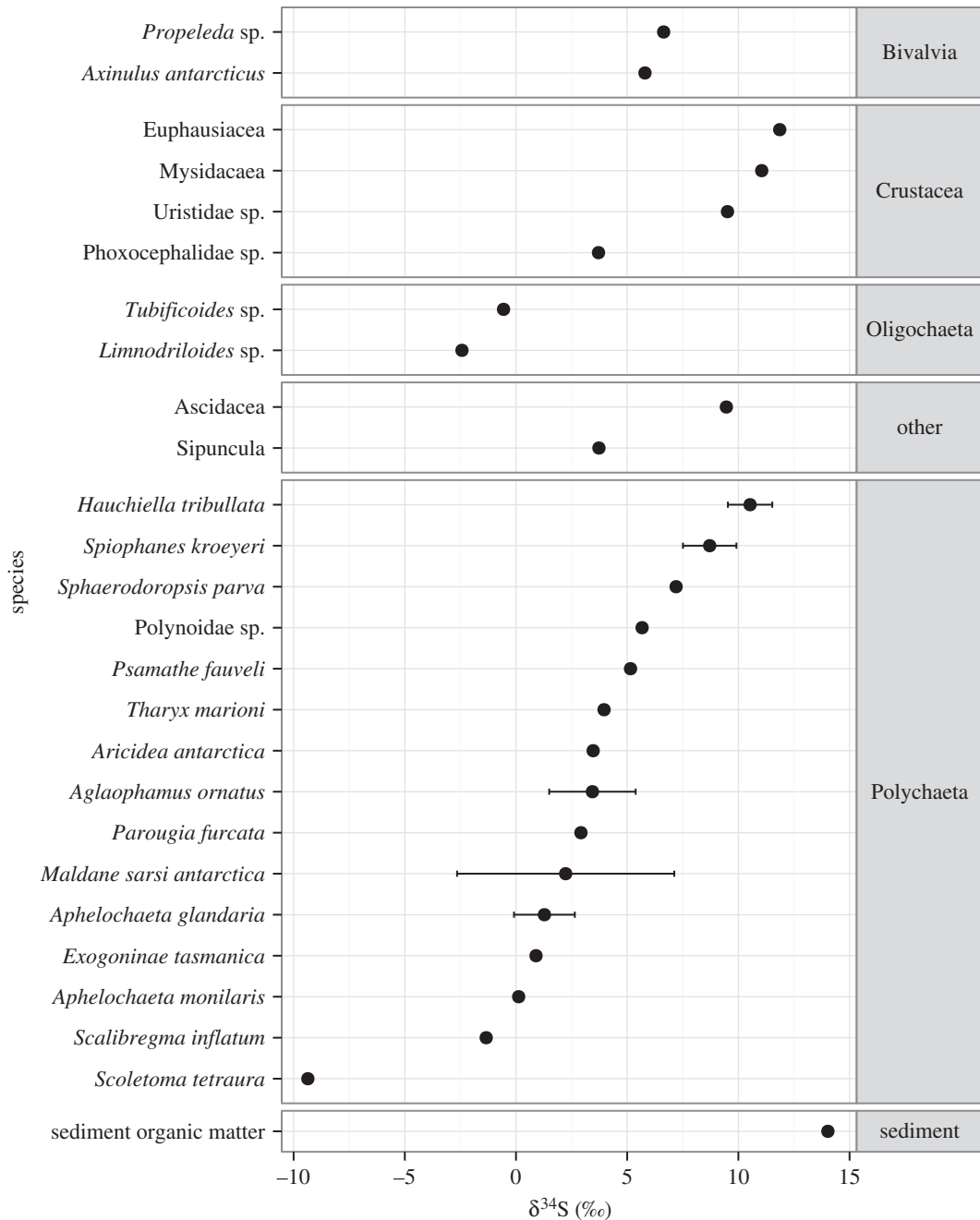


Figure 4. Faunal and Sediment organic matter $\delta^{34}\text{S} \pm 1 \text{ s.d.}$, grouped by higher taxa.

4.4. Geochemistry

Overall, downcore profiles are characterized by distinct geochemical zones indicative of early diagenesis (figure 5). A rapid downcore decrease in dissolved oxygen concentrations occurred in the top 0–2 cm, consistent with aerobic oxidation of organic material. Beneath the oxic layer (more than 1–2 cmbsf; figure 5), in the manganiferous and ferruginous zones, concentrations of dissolved Mn and Fe were elevated, reaching maximum concentrations of $2.4 \mu\text{mol kg}^{-1}$ and $110 \mu\text{mol kg}^{-1}$, respectively, at station 112. This is consistent with dissimilatory Fe and Mn reduction by microbial activity during organic matter remineralization. Organic carbon content was consistent downcore, ranging between 1.40 and 1.92%. Organic carbon $\delta^{13}\text{C}$ also did not show downcore changes (figure 5), varying by only approximately 1‰ throughout the entire profile.

Pore water concentrations of sulfate decreased downcore from the sediment surface, with concomitant increase in sulfide and TA in both the short megacores (figure 5) and the deeper gravity core samples

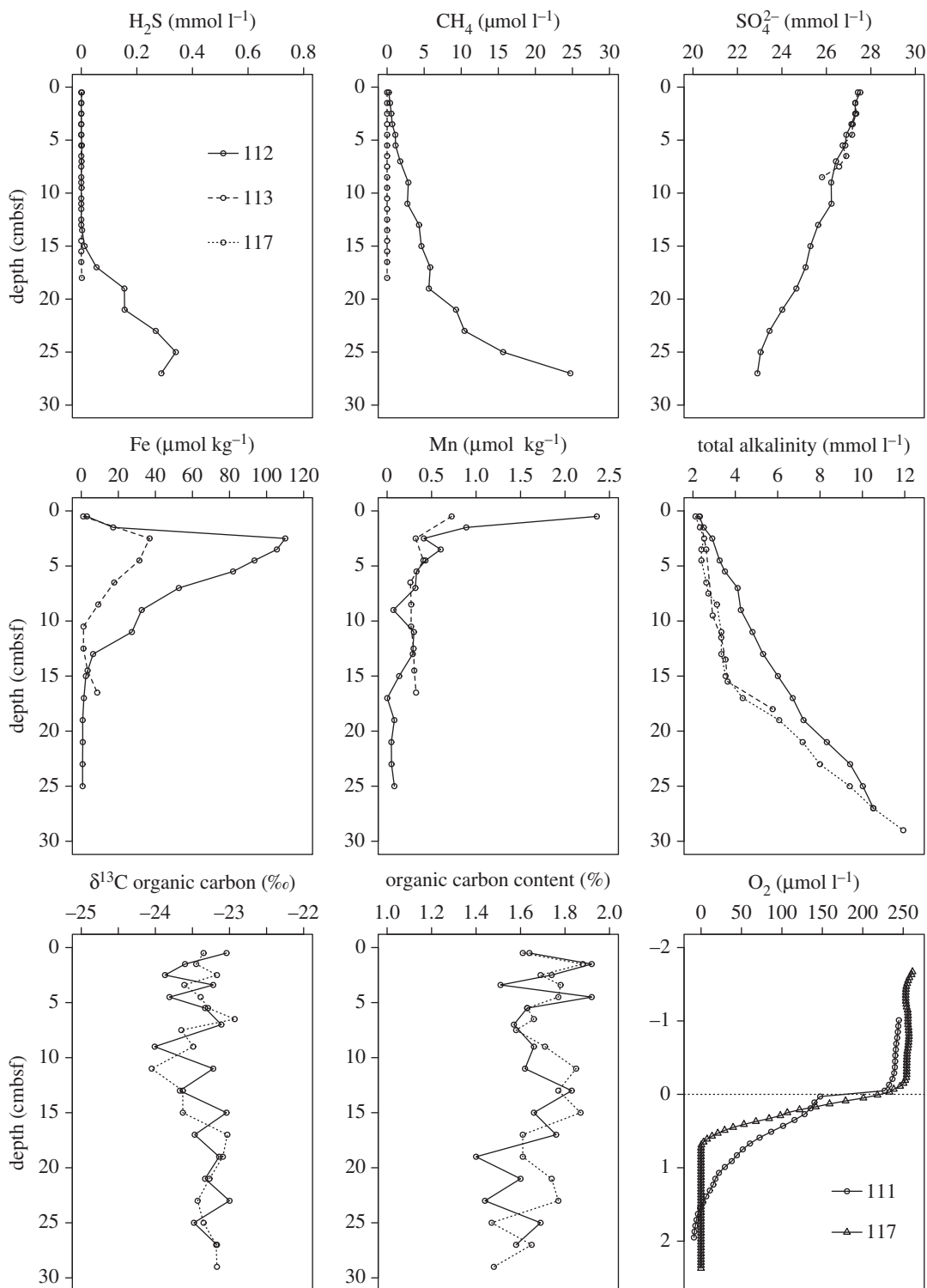


Figure 5. JC55 Megacore profiles. Legend as upper-left for all plots except oxygen (bottom-right).

(figure 6). The rapid increase in dissolved methane with depth, as observed in megacores JC55 112 and 117 below 20 cmbsf (figure 5), and particularly in deeper sections of the gravity core (approx. 140–160 cmbsf), are indicative of methane production at depth (figure 6).

4.5. Authigenic carbonates

XRD analysis of the superficially amorphous, brittle, yellow deposit on the valves of *Axinulus antarcticus* determined that these deposits were comprised predominately of the carbonates, aragonite and

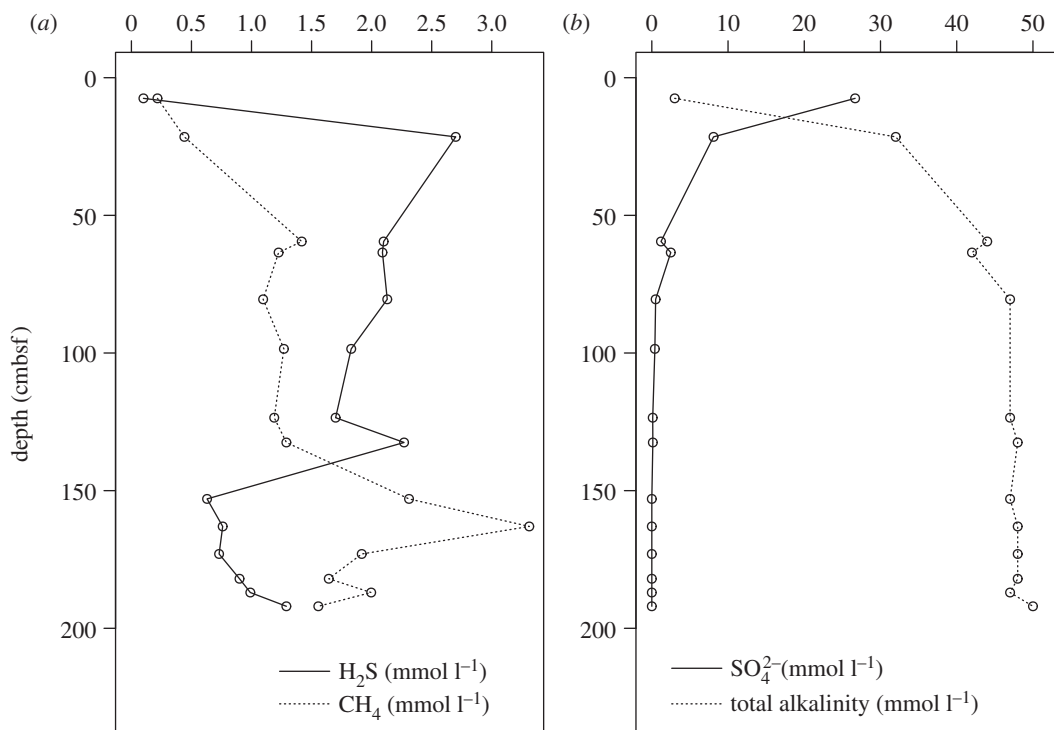


Figure 6. JC42 Gravity core profiles. X scale varies.

dolomite. A reference sample of freeze-dried sediment did not contain either of these carbonates and the strongest signal was of quartz. One shell deposit sample also contained small signals from mica and chlorite, presumably a contamination from surrounding sediment. Although the carbonate deposits were generally located on specific areas of shell (towards the dorsal margin), they were not consistent in shape and area, indicating that they were not precipitated as part of shell growth.

5. Discussion

5.1. Community composition

Cirratulid polychaetes were by far the most numerous of any macrofaunal family, comprising 27–45% of abundance. Although a cosmopolitan family of deep-sea polychaetes (source: OBIS), their presence has also been documented at several seeps [20,36,43,69], as well as oxygen minimum zones [69] and a sedimented vent in the Bransfield Strait [45]. The presence, and high abundance, of tubificid oligochaetes and thyasirid bivalves could be indicative of reducing conditions as both of these families are known from other methane seeps [36,37,73–78].

No differences were observed in assemblage composition between sites, indicating that the geochemical differences apparent in figure 5 were insufficient to influence assemblage structure. The density of *Aphelochaeta* spp., *Axinulus antarcticus* and tubificid oligochaetes accounted for 62–72% of the total and were consistently highly dominant, indicative of reducing conditions at all sites [36], supporting our suggestion of macrofaunal assemblages structured by sediment geochemistry. Faunal assemblages were compared with others from the West Antarctic Peninsula (WAP) and from seeps in the Pacific [68–70]. Assemblage composition was clearly different, at class/order level to the WAP and Pacific margin seeps (PERMANOVA, $p = 0.001$; figure 7) [70]. Polychaetes were the dominant class at the WAP and South Georgia (71.3 and 64.1%, respectively) but the South Georgia assemblages contained much higher proportions of oligochaetes and bivalves. Species-level discriminated polychaete assemblages from the WAP [70] showed very high dominance (26–70%) of a single spionid species, *Aurospio foodbanesia* [79] in contrast to the dominance of cirratulid polychaetes in South Georgia samples. Spionid polychaetes were comparatively absent from our sites (0.66% of total abundance, approx. 1% of polychaetes), represented almost entirely by *Spiophanes kroeyeri*. Samples from comparable depths (300–500 m) around the South Sandwich Islands [80] were different to the South Georgia assemblages,

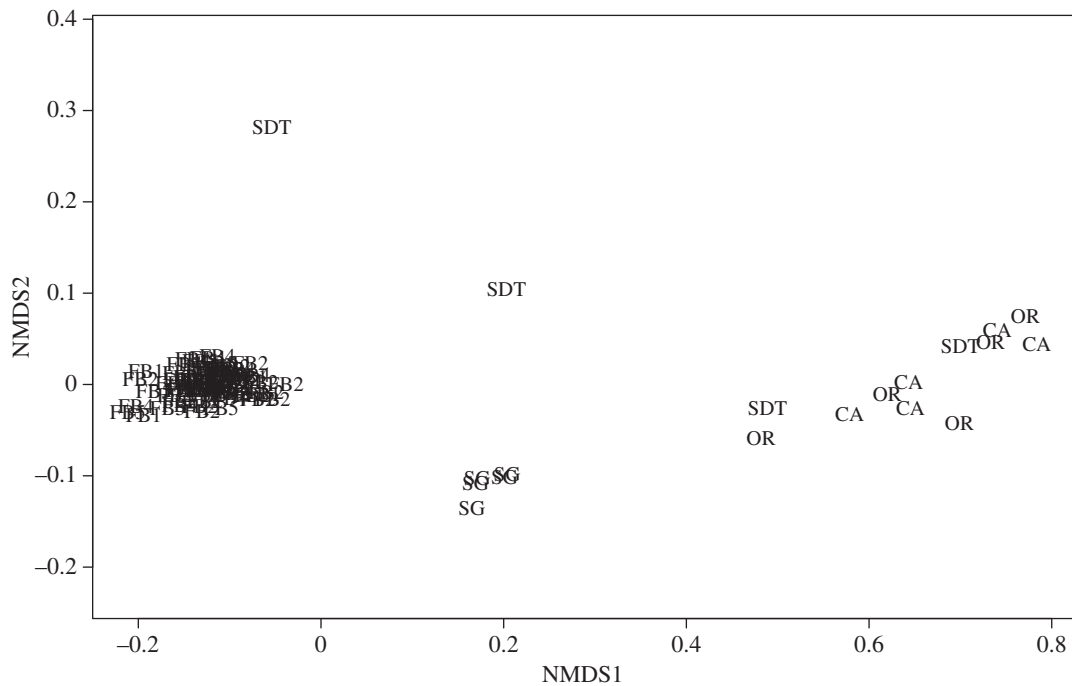


Figure 7. Class/Order level multidimensional scaling (MDS) plot of South Georgia macrofauna composition compared to cold seep and background sediments. CA, California margin seeps [69]; FB, FoodBancs, WAP [70]; OR, Oregon margin seeps [69]; SDT, San Diego Trough seeps [68]; SG, South Georgia (this study).

being instead dominated by molluscs and malacostracans, with annelids comprising a relatively small component of the assemblages. These samples, while not directly comparable owing to differences in sampling techniques (collected by epibenthic sled, as opposed to megacoring), provide evidence of differences between South Georgia and other shelf areas of the East Scotia back-arc basin at several taxonomic levels and support the suggestion that these sediments represent a continuum between seep and background sediments.

Remotely operated vehicles were deployed during JC42 (ROV *Isis*) and JC55 (Seabed High-Resolution Imaging Platform) and undertook visual surveys of areas of interest, as identified by shipboard echo sounders (EK60) and elevated methane levels in the water column, but no aggregations of microbial mat or seep-endemic fauna were observed [15,16]. Cold seep sites in the Sea of Okhotsk were also not inhabited by seep-endemic fauna shallower than 370 m depth [38] and so the absence of seep-endemic fauna from South Georgia sediments may reflect depth-related patterns in assemblage structure.

5.2. Trophic structure and carbon sources

Most metazoan isotope ratios were characteristic of sediment organic matter ($\delta^{13}\text{C}_{\text{org}} -23.40\text{‰}$), which is presumed to be predominately surface-derived OM, with limited *in situ* production. Estimates of the $\delta^{13}\text{C}$ signatures of surface particulate organic carbon (POC) at this latitude approximately range between -29 and -24‰ [81]. Even in *Axinulus antarcticus*, where authigenic carbonates suggestive of AOM were directly observed, $\delta^{13}\text{C}$ signatures of tissue were not indicative of assimilation of MDC (mean $\delta^{13}\text{C} -20.10\text{‰}$, figure 5). The lack of a strong MDC signal in metazoan tissue indicates that methanotrophy was not a significant contributor to the macrofaunal food web and we suggest that the methane flux was insufficient to support dense aggregations of methanotrophic bacteria at the sediment surface. This is similar to Californian seep sediments (depth 520 m) where macrofauna had an estimated 0–5% dietary contribution of MDC [30]. It is probable that, given the relatively high concentration of sulfate in the upper layers of the sediment and the relatively high rate of methane depletion between 20 and 30 cmbsf (figure 5), the majority of AOM activity occurred deeper than the range of the metazoans sampled here (0–10 cmbsf). This is consistent with the absence of microbial mats or aggregations of seep-endemic fauna observed during video transects of the area [13,15,16]. The sub-surface depletion of methane concentration (figure 5) emphasizes the role of microbial processes in sub-surface methane cycling, limiting potential atmospheric emissions.

Polychaetes of the order Phyllodocida (e.g. alciopids, hesionids, nephtyids and polynoids) were among the taxa with the highest $\delta^{15}\text{N}$ values (more than 9‰, figure 3), indicating that these taxa occupied a higher trophic level. These taxa are all characterized by high activity (large locomotory structures) and mouthparts capable of a predatory lifestyle. However, syllids (*Sphaerosyllis hirsuta* and *Exogoninae (parexogone) tasmanica*) that also possess morphology adapted to carnivory, did not have the same $\delta^{15}\text{N}$ enrichment (mean 6.12‰) and also had low $\delta^{13}\text{C}$ and $\delta^{34}\text{S}$ values (figure 3; [4]). This suggests that these taxa might have derived some of their organic matter from bacterial MDC, consistent with relatively low $\delta^{13}\text{C}$ and $\delta^{15}\text{N}$ values [21,29]. *Sphaerosyllis* and *Exogoninae* are common on carbonates at Costa Rica [43] and Hydrate Ridge seeps [82] and in Chile Margin hydrothermal sediments (Thurber *et al.* unpublished data, cited in [36]).

Interestingly, some of the highest $\delta^{15}\text{N}$ values belonged to tubificid oligochaetes (mean 10.58‰ \pm s.d. 0.28, figure 3) and an unidentified species of echiuran (mean 10.28‰ \pm s.d. 0.01, figure 3), consistent with observations of a morphologically similar species of echiuran at a sediment-hosted hydrothermal vent in the Bransfield Strait [49]. This may indicate selective feeding strategies that favour OM that had been recycled by microbial activity, resulting in a relatively high trophic level. A visual inspection of gut content of tubificid oligochaetes (400 \times magnification) did not identify any remains that could be attributed to specific food sources.

Sulfur isotope ratios were the most variable of the isotopic data, suggesting diverse feeding strategies between and within taxa (figure 4). Faunal and sediment $\delta^{34}\text{S}$ (Mean \pm s.d. 4.25 \pm 5.13 and 14.03‰ \pm 0.12, respectively) were also lower than might be expected of non-methane-enriched sediments (18–20‰ [83]), indicating the influence of a relatively ^{34}S -poor source. Low $\delta^{34}\text{S}$ values are associated with microbial AOM [24,31] as sulfate reduction, which results in low $\delta^{34}\text{S}$ signatures, co-occurs with methane oxidation. This suggests that microbial MDC was a component of the macrofaunal food web. Variability in $\delta^{34}\text{S}$ signatures was unsupported by carbon isotopic measurements, which showed relatively little variation and there is a clear disparity between carbon and sulfur isotope composition. This highlights the importance of using multiple SIA to elucidate trophodynamics. The disparity between sulfur and carbon isotopic measurements could have resulted from differences in carbon and sulfur processing within the biota or as a result of the highly variable isotopic fractionation associated with sulfate–sulfide exchanges (sulfate reduction and sulfide oxidation) [31]. Additionally, it is possible that the relative contribution of AOM to total organic carbon and total organic sulfur may have been different and thus contributing to the differences in ranges observed, though this cannot be assessed from the available data.

Sediment organic carbon $\delta^{13}\text{C}$ was generally lighter than most of the faunal measurements (difference in means $\delta^{13}\text{C}$ of 3.90‰; figure 3) and may have been a mix of surface-derived material and MDC. The relatively heavy faunal signatures probably resulted from a preservation/treatment effect rather than an additional, unknown source of organic matter. Isotopic shifts may have arisen from ethanol preservation or the fact that sediment organic carbon samples were acidified but faunal samples were not. Untreated sediment samples had $\delta^{13}\text{C}$ values that were 0.66‰ greater than acidified sediment samples [83]. Only faunal samples preserved in ethanol were selected to minimize any faunal preservation effects between different samples. However, ethanol preservation can still impact faunal signatures [84] although this effect can be very variable. A review of isotope shifts associated with preservation effects demonstrated that storing samples in more than 70% ethanol significantly increased or decreased carbon isotopic signatures in four of eight published studies. Nitrogen isotopic signatures were significantly affected in three out of five published studies. Given the variable response to ethanol preservation, it is difficult to correct isotopic signatures but it is likely that preservation effects may have artificially altered some individual faunal isotopic signatures.

5.3. Phospholipid fatty acids

Although it can be difficult to ascribe PLFAs to specific microbial groups or processes, some compounds are indicative of certain groups [56], especially when they occur in high relative abundance. For example, although the abundant PLFAs C16:1 ω 7c and C18:1 ω 7 may be synthesized by a number of groups, including phytoplankton and bacteria [55,58], they occurred in very high abundance in symbiont-bearing species at hydrothermal vents and seeps, and are linked to sulfide oxidation [61,85–89]. PLFAs attributed to sulfate reduction and sulfide oxidation at seeps [86] accounted for 9.3 and 27.7% of the total abundance respectively. Biomarkers specific to phytoplankton groups, like 20:5 ω 3 in diatoms [90], occurred in relatively low abundance (approx. 5% of the total) though this is not to say that the contribution of photosynthetically derived OM was this low, since other PLFAs are likely to have

come from phytoplankton [55,90]. Photosynthetic PLFAs will also have decayed during sinking and are inevitably underestimated in such samples.

MUFAs in particular are associated with cold seeps [35,54,56,87] and three of the four most abundant FAs were MUFAs, collectively accounting for 41.24% of the total composition. While these FAs may not be exclusive to methanotrophic bacteria [55], their high relative abundance is evidence of active (or very recently active) methanotrophy in the upper layers of sediment (0–1 cm). Carbon isotopic signatures of PLFAs were generally quite similar to those of reducing sediments in the Gulf of Mexico [91]. MUFA $\delta^{13}\text{C}$ ranged between -30.73 and -24.55‰ suggesting either a very heavy source of methane (compared with biogenic methane), or that these FAs were produced from a combination of methanotrophy and heterotrophic metabolism. Methane with similarly heavy isotopic values is more commonly associated with a hydrothermal origin [92], hence it is unlikely that methane was the sole source of carbon in MUFAs without a very substantial metabolic fractionation effect.

5.4. Geochemistry

Sulfate showed a steep decline between 0 and 50 cmbsf (figure 6), and there was a concomitant increase in H_2S and alkalinity indicating sulfate reduction was active at these depths. The fact that the sulfate depletion was accompanied by an increase in pore water methane concentrations with depth suggests that AOM may have been active. The sulfate depletion is relatively rapid compared with methane-containing slope sediments on the Norwegian, Gulf of Mexico, Chilean and Argentine margins, where complete depletion of sulfate did not occur above 100, 250, 350 and 400 cmbsf, respectively [4,93–95]. These sites generally had comparable or higher methane concentrations below the sulfate reduction zone than the South Georgia shelf. These pore water profiles were similar to other sediments where AOM has been directly observed but the approximate depth of complete sulfate depletion was shallower on the South Georgia shelf than elsewhere [4,93,94]. Sediments with little to no methane flux showed very little decline in pore water sulfate concentrations in the top 5 m of sediment [93]. Oxygen penetration depth (figure 5) was less than 2 cmbsf, suggesting that aerobic oxidation of methane was probably very limited.

Despite a relatively steep depletion in methane concentrations between approximately 20 and 30 cmbsf, we did not observe a change in the $\delta^{13}\text{C}$ of sediment organic carbon (figure 5) that might have resulted from significant rates of methanotrophy. This was probably owing to the small quantities of pore water methane relative to the total mass of organic carbon. We estimate that, if entirely converted into POC, this amount of methane would only have changed the $\delta^{13}\text{C}_{\text{org}}$ by between 10^{-2} and 10^{-14}‰ in each core section, depending upon the isotopic signature of the methane which was unknown, but estimated between approximately -80 and -50‰ [96]. This potential change is far less than is observable, given the variability in the data and is comparable to $\delta^{13}\text{C}_{\text{org}}$ profiles at Gulf of Mexico cold seeps [97].

5.5. Authigenic carbonates

Authigenic carbonates have been widely documented at methane seeps, since AOM increases the concentration of bicarbonate in pore waters (figure 5; [6]) and favours *in situ* precipitation [24,49,98–100]. Carbonate production at methane seeps can result in several different forms, both low- and high-Mg content, including calcite, aragonite, dolomite and ikaite [2,43,101–103] and samples of ikaite were previously found on the southwest South Georgia margin [41]. Our observations were of small, localized carbonate crusts on the shells of *Axinulus antarcticus*, but not on other bivalve species or in the ambient sediment from the area. These observations are in contrast with previous descriptions of large carbonate precipitations within the sediment reported at other seeps [2,42,104–107].

Exterior calcification or encrusting material is known from other bivalve species. For example, some species in the family Veneridae precipitate micrometre scale, needle-shaped, aragonite formations on their periostracum [106,108]. Lucinid species, known from chemosynthetic ecosystems, can also precipitate unusual periostracal features, as arrays of scales [109]. Inspection of *A. antarcticus* and other bivalve species present (e.g. *Propeleda* sp. Nuculanidae) under a scanning electron microscope did not reveal similar structures (electronic supplementary material, S4).

Mineral deposits have also been associated with *Montacuta ferruginosa* (Montagu, Montacutidae), in this case a phosphorus-rich ferric mineral that forms part of an epibiotic biofilm [110]. These deposits were attributed to a γ -proteobacterial community, using iron, and were not linked to methanotrophy or AOM, but were similar to hydrothermal vent communities [111–113]. Microbial compositional data were not available here but given the elevated levels of methane, the AOM-associated carbonates present

and the low $\delta^{34}\text{S}$ signature of *Aximulus* (relative to sediment), it seems likely that these precipitates were also microbially mediated [113]. We suggest that the feeding behaviour of *A. antarcticus* enhances local fluid flow and thus favours precipitation of carbonates, potentially facilitated by a consortia of anaerobic methanotrophic bacteria [106].

5.6. Conclusion

Macrofaunal assemblage composition was indicative of reducing conditions but the incorporation of MDC was apparently very limited to both microbial and metazoan assemblages, similar to off-seep and near-seep areas from other studies. We highlight a disparity between carbon and sulfur isotopic measurements that emphasizes the need to use multiple isotopes in the study of trophodynamics in chemosynthetic ecosystems. Geochemical signatures were consistent with weak methane seepage and we demonstrate the role of sub-seafloor methane consumption, preventing methane emissions into the bottom water.

Ethics. In accordance with the Antarctic Act (1994) and the Antarctic Regulations (1995), necessary permits (S5-4/2010) were acquired from the South Georgia and South Sandwich Islands Government.

Data accessibility. The data presented in this paper are accessible as electronic supplementary material that accompanies this article.

Authors' contributions. Conceived and executed the sampling programme at sea: A.A., C.W., A.G.G., W.D.K.R., L.E.H. and R.A.M. Geochemical analyses: A.A., L.E.H., R.A.M. and J.B.B. Taxonomic analyses: J.B.B., A.G.G. and C.T.S.L. Isotopic analyses: J.B.B., C.W., W.D.K.R. and J.N. Elemental analyses: C.T.S.L. and J.B.B. Statistical methods: J.B.B. Wrote the paper: J.B.B. and A.A. Produced plots: J.B.B. Commented on and approved the paper: J.B.B., A.A., C.W., A.G.G., C.T.S.L., W.D.K.R., L.E.H., J.N. and R.A.M.

Competing interests. This work was supported entirely by the Natural Environment Research Council. NERC Staff were not involved in the study design, manuscript preparation or decision to publish. All authors declare that there are no conflicts of interest arising from the work presented here.

Funding. This work was funded by the NERC ChEsSo consortium (Chemosynthetically driven Ecosystems South of the Polar Front, NERC grant no. NE/DOI249X/I). C.W. was supported by a bursary from Antarctic Science Ltd. J.B.B. was funded by a NERC PhD Studentship (NE/L501542/1). Isotopic analyses were funded by the NERC Life Sciences Mass Spectrometry Facility (EK246-01/15).

Acknowledgements. The authors would like to thank the following for their support in this work. We thank the Masters and Crews of RRS *James Clark Ross* cruise 224 and RRS *James Cook* cruises 042 and 055 for technical support and the Cruise Principal Scientific Officers; Prof. Alex Rogers and Prof. Paul Tyler. We also thank the editor and anonymous reviewers for their valuable contributions and assistance. We gratefully acknowledge taxonomic contributions from P. Graham Oliver and Christer Erséus. We also thank: Christopher Sweeting for his assistance in preparing the mass spectrometry grant application and curation of the megafaunal samples; Lesley Neve for the processing and analysis of XRD samples and Barry Thornton for processing and analysis of PLFA samples.

References

- Klauda JB, Sandler SI. 2005 Global distribution of methane hydrate in ocean sediment. *Energy Fuels* **19**, 459–470. (doi:10.1021/ef049798o)
- Naehr TH, Eichhubl P, Orphan VJ, Hovland M, Paull CK, Ussler W, Lorenson TD, Greene HG. 2007 Authigenic carbonate formation at hydrocarbon seeps in continental margin sediments: a comparative study. *Deep Sea Res. II Top. Stud. Oceanogr.* **54**, 1268–1291. (doi:10.1016/j.dsr2.2007.04.010)
- Wright JD, Schaller MF. 2013 Evidence for a rapid release of carbon at the Palaeocene-Eocene thermal maximum. *Proc. Natl Acad. Sci. USA* **110**, 15 908–15 913. (doi:10.1073/pnas.1309188110)
- Knab NJ, Cragg BA, Borowski C, Parkes RJ, Pancost R, Jørgensen BB. 2008 Anaerobic oxidation of methane (AOM) in marine sediments from the Skagerrak (Denmark). I. Geochemical and microbiological analyses. *Geochim. Cosmochim. Acta* **72**, 2868–2879. (doi:10.1016/j.gca.2008.03.016)
- Hinrichs KU, Boetius A. 2002 The anaerobic oxidation of methane: new insights in microbial ecology and biogeochemistry. In *Ocean margin systems* (eds G Wefer, D Billett, BB Jørgensen, M Schlüter, T van Weering), pp. 457–477. Heidelberg, Germany: Springer.
- Krüger M, Treude T, Wolters H, Nauhaus K, Boetius A. 2005 Microbial methane turnover in different marine habitats. *Palaeogeogr. Palaeoclimatol. Palaeoecol.* **227**, 6–17. (doi:10.1016/j.palaeo.2005.04.031)
- Geletti R, Busetti M. 2011 A double bottom simulating reflector in the western Ross Sea, Antarctica. *J. Geophys. Res.* **116**, B04101. (doi:10.1029/2010JB007864)
- Hart PE, Pohlman JW, Lorenson TD, Edwards BD (eds). 2011 Beaufort Sea deep-water gas hydrate recovery from a seafloor mound in a region of widespread BSR occurrence. In *Proc. of the 7th Int. Conf. on Gas Hydrates, Edinburgh, UK, 17–21 July*. USGS Publications.
- Lodolo E, Camerlenghi A, Brancolini G. 1993 A bottom simulating reflector on the South Shetland margin, Antarctic Peninsula. *Antarct. Sci.* **5**, 207–210. (doi:10.1017/S0954102093000264)
- Römer M et al. 2014 First evidence of widespread active methane seepage in the Southern Ocean, off the sub-Antarctic island of South Georgia. *Earth Planet. Sci. Lett.* **403**, 166–177. (doi:10.1016/j.epsl.2014.06.036)
- Hauquier F, Ingels J, Gutt J, Raes M, Vanreusel A. 2011 Characterisation of the nematode community of a low-activity cold seep in the recently ice-shelf free Larsen B area, Eastern Antarctic Peninsula. *PLoS ONE* **6**, e22240. (doi:10.1371/journal.pone.0022240)
- Kvenvolden KA, Golan-Bac M, Rapp JB. 1987 Hydrocarbon geochemistry of sediments offshore from Antarctica: Wilkes Land Continental Margin. *CPECEM Earth Sci. Series* **5A**, 205–213.
- Larter RD et al. 2009 RRS James Clark Ross Cruise JR224: Chemosynthetically-driven Ecosystems

- South of the Polar Front consortium programme. BODC Cruise Report. (https://www.bodc.ac.uk/data/information_and_inventories/cruise_inventory/report/jr224.pdf)
14. Lodolo E, Camerlenghi A, Madrusani G, Tinivella U, Rossi G. 2002 Assessment of gas hydrate and free gas distribution on the South Shetland margin (Antarctica) based on multichannel seismic reflection data. *Geophys. J. Int.* **148**, 103–119. (doi:10.1046/j.0956-540x.2001.01576.x)
 15. Rogers AD *et al.* 2010 RRS James Cook Cruise 42: Chemosynthetic Ecosystems of the Southern Ocean. BODC Cruise Report. (https://www.bodc.ac.uk/data/information_and_inventories/cruise_inventory/report/jc042.pdf)
 16. Tyler PA *et al.* 2011 RRS James Cook Cruise JC55: Chemosynthetic Ecosystems of the Southern Ocean. BODC Cruise Report. (https://www.bodc.ac.uk/data/information_and_inventories/cruise_inventory/report/jc055.pdf)
 17. Wood WT, Jung WY (eds). 2008 Modeling the extent of the Earth's methane hydrate cryosphere. In *Proc. of the 6th Int. Conf. on Gas Hydrates, Vancouver, BC, Canada, 6–10 July*. University of British Columbia.
 18. Levin LA. 2005 Ecology of cold seep sediments: interactions of fauna with flow, chemistry and microbes. *Oceanogr. Mar. Biol. Annu. Rev.* **43**, 1–46. (doi:10.1201/9781420037449.ch1)
 19. Levin LA *et al.* 2016 Hydrothermal vents and methane seeps: rethinking the sphere of influence. *Front. Mar. Sci.* **3**, 72. (doi:10.3389/fmars.2016.00072)
 20. Levin LA, Mendoza GF. 2007 Community structure and nutrition of deep methane-seep macrobenthos from the North Pacific (Aleutian) Margin and the Gulf of Mexico (Florida Escarpment). *Mar. Ecol. Prog. Ser.* **28**, 131–151. (doi:10.1111/j.1439-0485.2006.00131.x)
 21. Thurber AR, Kröger K, Neira C, Wiklund H, Levin LA. 2010 Stable isotope signatures and methane use by New Zealand cold seep benthos. *Mar. Ecol. Prog. Ser.* **272**, 260–269. (doi:10.1016/j.margeo.2009.06.001)
 22. Boetius A *et al.* 2000 A marine microbial consortium apparently mediating anaerobic oxidation of methane. *Nature* **407**, 623–626. (doi:10.1038/35036572)
 23. Boetius A, Suess E. 2004 Hydrate Ridge: a natural laboratory for the study of microbial life fueled by methane from near-surface gas hydrates. *Chem. Geol.* **205**, 291–310. (doi:10.1016/j.chemgeo.2003.12.034)
 24. Habicht KS, Canfield DE. 1997 Sulfur isotope fractionation during bacterial sulfate reduction in organic-rich sediments. *Geochim. Cosmochim. Acta* **61**, 5351–5361. (doi:10.1016/S0016-7037(97)00311-6)
 25. Hinrichs KU, Hayes JM, Sylva SP, Brewer PG, DeLong EF. 1999 Methane-consuming archaeobacteria in marine sediments. *Nature* **398**, 802–805. (doi:10.1038/19751)
 26. Levin LA, Ziebis W, Mendoza GF, Bertics VJ, Washington T, Gonzalez J, Thurber AR, Ebbe B, Lee RW. 2013 Ecological release and niche partitioning under stress: Lessons from dorvilleid polychaetes in sulfidic sediments at methane seeps. *Deep-Sea Res. II Top. Stud. Oceanogr.* **92**, 214–233. (doi:10.1016/j.dsr2.2013.02.006)
 27. Levin LA, Ziebis W, Mendoza GF, Growney VA, Tryon MD, Brown KM, Mahn C, Gieskes JM, Rathburn AE. 2003 Spatial heterogeneity of macrofauna at northern California methane seeps: influence of sulfide concentration and fluid flow. *Mar. Ecol. Progress Ser.* **265**, 123–139. (doi:10.3354/meps265123)
 28. Levin LA, Ziebis W, Mendoza GF, Growney-Cannon V, Walther S. 2006 Recruitment response of methane-seep macrofauna to sulfide-rich sediments: an in situ experiment. *J. Exp. Mar. Biol. Ecol.* **330**, 132–150. (doi:10.1016/j.jembe.2005.12.022)
 29. Levin LA, Mendoza GF, Konotchick T, Lee R. 2009 Macrobenthos community structure and trophic relationships within active and inactive Pacific hydrothermal sediments. *Deep Sea Res. II Top. Stud. Oceanogr.* **56**, 1632–1648. (doi:10.1016/j.dsr2.2009.05.010)
 30. Levin LA, Michener RH. 2002 Isotopic evidence for chemosynthesis-based nutrition of macrobenthos: the lightness of being at Pacific methane seeps. *Limnol. Oceanogr.* **47**, 1336–1345. (doi:10.4319/lo.2002.47.5.1336)
 31. Canfield DE. 2001 Isotope fractionation by natural populations of sulfate-reducing bacteria. *Geochim. Cosmochim. Acta* **65**, 1117–1124. (doi:10.1016/S0016-7037(00)00584-6)
 32. Peterson BJ. 1999 Stable isotopes as tracers of organic matter input and transfer in benthic food webs: a review. *Acta Oecol. Int. J. Ecol.* **20**, 479–487. (doi:10.1016/S1146-609X(99)00120-4)
 33. Boschker HT, Middelburg JJ. 2002 Stable isotopes and biomarkers in microbial ecology. *FEMS Microbiol. Ecol.* **40**, 85–95. (doi:10.1111/j.1574-6941.2002.tb00940.x)
 34. Boschker HT, Nold SC, Wellsbury P, Bos D, de Graaf W, Pel R, Parkes RJ, Cappenberg TE. 1998 Direct linking of microbial populations to specific biogeochemical processes by ¹³C-labelling of biomarkers. *Nature* **392**, 801–805. (doi:10.1038/33900)
 35. Colaço A, Desbruyères D, Guezennec J. 2007 Polar lipid fatty acids as indicators of trophic associations in a deep-sea vent system community. *Mar. Ecol. Prog. Ser.* **28**, 15–24. (doi:10.1111/j.1439-0485.2006.00123.x)
 36. Bernardino AF, Levin LA, Thurber AR, Smith CR. 2012 Comparative composition, diversity and trophic ecology of sediment macrofauna at vents, seeps and organic falls. *PLoS ONE* **7**, e33515. (doi:10.1371/journal.pone.0033515)
 37. Dando PR, Bussmann J, Niven SJ, O'Hara SCM, Schmaljohann R, Taylor LJ. 1994 A methane seep area in the Skagerrak, the habitat of the pogonophore *Siboglinum poseidoni* and the bivalve mollusc *Thyasira sarsi*. *Mar. Ecol. Progress Ser.* **107**, 157–167. (doi:10.3354/meps107157)
 38. Sahling H, Galkin SV, Salyuk A, Greinert J, Foerstel H, Piepenburg D, Suess E. 2003 Depth-related structure and ecological significance of cold-seep communities: a case study from the Sea of Okhotsk. *Deep-Sea Res. I Oceanogr. Res. Pap.* **50**, 1391–1409. (doi:10.1016/j.dsr.2003.08.004)
 39. Piñero E, Marquardt M, Hensen C, Haeckel M, Wallmann K. 2013 Estimation of the global inventory of methane hydrates in marine sediments using transfer functions. *Biogeosciences* **10**, 959–975. (doi:10.5194/bg-10-959-2013)
 40. Pohlman JW, Riedel M, Bauer JE, Canuel EA, Paull CK, Lapham L, Grabowski KS, Coffin RB, Spence GD. 2013 Anaerobic methane oxidation in low-organic content methane seep sediments. *Geochim. Cosmochim. Acta* **108**, 184–201. (doi:10.1016/j.gca.2013.01.022)
 41. Belchier M *et al.* 2004 FPRV Dorada cruise DOSG04: South Georgia Groundfish Survey, 6th January–10th February 2004. A report to the Government of South Georgia and the South Sandwich Islands.
 42. Greinert J, Derkachev A. 2004 Glendonites and methane-derived Mg-calcites in the Sea of Okhotsk, Eastern Siberia: implications of a venting-related ikaite/glendonite formation. *Mar. Ecol. Prog. Ser.* **204**, 129–144. (doi:10.1016/S0025-3227(03)00354-2)
 43. Levin LA, Mendoza GF, Grupe BM, Gonzalez JP, Jellison B, Rouse G, Thurber AR, Waren A. 2015 Biodiversity on the rocks: macrofauna inhabiting authigenic carbonate at Costa Rica methane seeps. *PLoS ONE* **10**, e0131080. (doi:10.1371/journal.pone.0131080)
 44. Gage JD, Bett BJ. 2005 Deep-sea benthic sampling. In *Methods for the study of the marine benthos* (eds NA Holmes, AD McIntyre), pp. 273–319. Oxford, UK: Blackwell Scientific Publications.
 45. Bell JB, Wouds C, Brown LE, Little CTS, Sweeting CJ, Reid WDK, Little CTS, Glover AG. 2016 Macrofaunal ecology of sedimented hydrothermal vents in the Bransfield Strait, Antarctica. *Front. Mar. Sci.* **3**, 32.
 46. Jackson AL, Inger R, Parnell AC, Bearhop S. 2011 Comparing isotopic niche widths among and within communities: SIBER – Stable Isotope Bayesian Ellipses in R. *J. Anim. Ecol.* **80**, 595–602. (doi:10.1111/j.1365-2656.2011.01806.x)
 47. Parnell AC, Inger R, Bearhop S, Jackson AL. 2010 Source partitioning using stable isotopes: coping with too much variation. *PLoS ONE* **5**, e9672. (doi:10.1371/journal.pone.0009672)
 48. Connelly RM, Schlacher TA. 2013 Sample acidification significantly alters stable isotope ratios of sulfur in aquatic plants and animals. *Mar. Ecol. Progress Ser.* **493**, 1–8. (doi:10.3354/meps10560)
 49. Bell JB, Reid WDK, Pearce DA, Glover AG, Sweeting CJ, Newton J, Wouds C. In press. Hydrothermal activity lowers trophic diversity in Antarctic sedimented hydrothermal vents. *Biogeosciences*. (doi:10.5194/bg-2016-318)
 50. Reid WDK, Sweeting CJ, Wigham BD, Zwirgmaier K, Hawkes JA, McGill RAR, Linse K, Polunin NVC. 2013 Spatial differences in East Scotia Ridge hydrothermal vent food webs: influences of chemistry, microbiology and predation on trophodynamics. *PLoS ONE* **8**, e65563. (doi:10.1371/journal.pone.0065563)
 51. Main CE, Ruhl HA, Jones DOB, Yool A, Thornton B, Mayor DJ. 2015 Hydrocarbon contamination affects deep-sea benthic oxygen uptake and microbial community composition. *Deep Sea Res. I Oceanogr.*

- Res. Pap.* **100**, 79–87. (doi:10.1016/j.dsr.2014.12.008)
52. Bligh EG. 1959 A rapid method of total lipid extraction and purification. *Can. J. Biochem. Physiol.* **37**, 911–917. (doi:10.1139/o59-099)
 53. Thornton B, Zhang Z, Mayes RW, Högberg MN, Midwood AJ. 2011 Can gas chromatography combustion isotope ratio mass spectrometry be used to quantify organic compound abundance? *Rapid Commun. Mass Spectrom.* **25**, 2433–2438. (doi:10.1002/rcm.5148)
 54. Comeault A, Stevens CJ, Juniper SK. 2015 Mixed photosynthetic-chemosynthetic diets in vent obligate macroinvertebrates at shallow hydrothermal vents on Volcano 1, South Tonga Arc: evidence from stable isotope and fatty acid analyses. *Cahiers Biol. Mar.* **51**, 351–359.
 55. Dijkman NA, Boschker HTS, Stal LJ, Kromkamp JC. 2010 Composition and heterogeneity of the microbial community in a coastal microbial mat as revealed by the analysis of pigments and phospholipid-derived fatty acids. *J. Sea Res.* **63**, 62–70. (doi:10.1016/j.seares.2009.10.002)
 56. Kharlamenko VI, Zhukova NV, Khotimchenko SV, Svetashev VI, Kamenev GM. 1995 Fatty-acids as markers of food sources in a shallow-water hydrothermal ecosystem (Kraternaya Bight, Yankich island, Kurile Islands). *Mar. Ecol. Progress Ser.* **120**, 231–241. (doi:10.3354/meps120231)
 57. Kohring L, Ringelberg D, Devereux R, Stahl DA, Mittelman MW, White DC. 1994 Comparison of phylogenetic relationships based on phospholipid fatty acid profiles and ribosomal RNA sequence similarities among dissimilatory sulfate-reducing bacteria. *FEMS Microbiol. Lett.* **119**, 303–308. (doi:10.1111/j.1574-6968.1994.tb06905.x)
 58. Kunihiro T *et al.* 2014 Phospholipid-derived fatty acids and quinones as markers for bacterial biomass and community structure in marine sediments. *PLoS ONE* **9**, e96219. (doi:10.1371/journal.pone.0096219)
 59. Pond DW, Bell MV, Dixon DR, Fallick AE, Segonzac M, Sargent JR. 1998 Stable-carbon-isotope composition of fatty acids in hydrothermal vent mussels containing methanotrophic and thiotrophic bacterial endosymbionts. *Appl. Environ. Microbiol.* **64**, 370–375.
 60. Pond DW, Tarling GA, Mayor DJ. 2014 Hydrostatic pressure and temperature effects on the membranes of a seasonally migrating marine copepod. *PLoS ONE* **9**, e111043. (doi:10.1371/journal.pone.0111043)
 61. Pranal V, Fiala-Médioni A, Guezennec J. 1996 Fatty acid characteristics in two symbiotic gastropods from a deep hydrothermal vent of the west Pacific. *Mar. Ecol. Progress Ser.* **142**, 175–184. (doi:10.3354/meps142175)
 62. Reeburgh WS. 2007 Oceanic methane biogeochemistry. *Chem. Rev.* **107**, 486–513. (doi:10.1021/cr050362v)
 63. Sahling H, Wallman K, Dähmann A, Schmaljohann R, Petersen S. 2005 The physicochemical habitat of *Sclerolinum* sp. at Hook Ridge hydrothermal vent, Bransfield Strait, Antarctica. *Limnol. Oceanogr.* **50**, 598–606. (doi:10.4319/lo.2005.50.2.0598)
 64. Ivanenkov V, Lyakhin Y. 1978 Determination of total alkalinity in seawater. In *Methods of hydrochemical investigations in the ocean* (eds OK Borodovsky, V Ivanenkov), pp. 110–114. Moscow, Russia: Nauka Publishing House.
 65. Grasshoff L, Ehrhardt M, Kremling K, Anderson L. 1999 *Methods of seawater analysis*. Weinheim, Germany: Wiley-VCH.
 66. R Core Team. 2013 R: A Language and environment for statistical computing. Vienna, Austria: R Foundation for Statistical Computing. (<http://www.R-project.org/>)
 67. Oksanen J. 2013 *Multivariate analysis of ecological communities in R: vegan tutorial*. Vegan: Community Ecology Package. (<https://cran.r-project.org/web/packages/vegan/vegan.pdf>)
 68. Grupe BM, Krach ML, Pasulka AL, Maloney JM, Levin LA, Frieder CA. 2015 Methane seep ecosystem functions and services from a recently discovered southern California seep. *Mar. Ecol. Prog. Ser.* **36**, 91–108. (doi:10.1111/maec.12243)
 69. Levin LA, Mendoza GF, Gonzalez JP, Thurber AR, Cordes EE. 2010 Diversity of bathyal macrofauna on the northeastern Pacific margin: the influence of methane seeps and oxygen minimum zones. *Mar. Ecol. Prog. Ser.* **31**, 94–110. (doi:10.1111/j.1439-0485.2009.00335.x)
 70. Neal L, Mincks Hardy SL, Smith CR, Glover AG. 2011 Polychaete species diversity on the West Antarctic Peninsula deep continental shelf. *Mar. Ecol. Progress Ser.* **428**, 119–134. (doi:10.3354/meps09012)
 71. Anderson MJ. 2001 A new method for non-parametric multivariate analysis of variance. *Austral Ecol.* **26**, 32–46.
 72. Colwell RK. 2013 *EstimateS: statistical estimation of species richness and shared species from samples*. Version 9. (<http://purl.oclc.org/estimates>)
 73. Dando PR, Spiro B. 1993 Varying nutritional dependence of the chemo-autotrophic symbiotic bacteria, demonstrated by isotope ratios of tissue carbon and shell carbonate. *Mar. Ecol. Progress Ser.* **92**, 151–158. (doi:10.3354/meps092151)
 74. Engel AS. 2007 Observations on the biodiversity of sulfidic karst habitats. *J. Cave Karst Stud.* **69**, 187–206.
 75. Fujiwara Y, Kato C, Masui N, Fujikura K, Kojima S. 2001 Dual symbiosis in the cold-seep thyasirid clam *Maoritithys hadalis* from the hadal zone in the Japan Trench, western Pacific. *Mar. Ecol. Progress Ser.* **214**, 151–159. (doi:10.3354/meps214151)
 76. Giere O, Krieger J. 2001 A triple bacterial endosymbiosis in a gutless oligochaete (Annelida): ultrastructural and immunocytochemical evidence. *Invertebr. Biol.* **120**, 41–49. (doi:10.1111/j.1744-7410.2001.tb00024.x)
 77. Oliver PG, Holmes AM. 2006 New species of Thyasiridae (Bivalvia) from chemosynthetic communities in the Atlantic Ocean. *J. Conchol.* **39**, 175–183.
 78. Oliver PG, Sellanes J. 2005 New species of Thyasiridae from a methane seepage area off Concepción, Chile. *Zootaxa*. **1092**, 1–20.
 79. Mincks SL, Dyal PL, Paterson GLJ, Smith CR, Glover AG. 2009 A new species of *Aurospio* (Polychaeta, Spionidae) from the Antarctic shelf, with analysis of its ecology, reproductive biology and evolutionary history. *Mar. Ecol. Prog. Ser.* **30**, 181–197. (doi:10.1111/j.1439-0485.2008.00265.x)
 80. Kaiser S, Barnes DKA, Linse K, Brandt A. 2008 Epibenthic macrofauna associated with the shelf and slope of a young and isolated Southern Ocean island. *Antarct. Sci.* **20**, 281–290. (doi:10.1017/S0954102008001107)
 81. Young JN, Bruggeman J, Rickaby REM, Erez J, Conte M. 2013 Evidence for changes in carbon isotopic fractionation by phytoplankton between 1960 and 2010. *Glob. Biogeochem. Cycles* **27**, 505–515. (doi:10.1002/gbc.20045)
 82. Levin LA, Mendoza GF, Grupe BM. In press. Methane seepage effects on biodiversity and biological traits of macrofauna inhabiting authigenic carbonates. *Deep Sea Res. II Top. Stud. Oceanogr.*
 83. Reid WDK, Wigham BD, McGill RAR, Polunin NVC. 2012 Elucidating trophic pathways in benthic deep-sea assemblages of the Mid-Atlantic Ridge north and south of the Charlie-Gibbs Fracture Zone. *Mar. Ecol. Progress Ser.* **463**, 89–103. (doi:10.3354/meps09863)
 84. Barrow LM, Bjorndal KA, Reich KJ. 2008 Effects of preservation method on stable carbon and nitrogen isotope values. *Physiol. Biochem. Zool.* **81**, 688–693. (doi:10.1086/588172)
 85. Riou V, Bouillon S, Serrão Santos R, Dehairs F, Colaço A. 2010 Tracing carbon assimilation in endosymbiotic deep-sea hydrothermal vent Mytilid fatty acids by ¹³C-fingerprinting. *Biogeochemistry* **7**, 2591–2600. (doi:10.5194/bg-7-2591-2010)
 86. Li Y, Peacock A, White D, Geyer R, Zhang C. 2007 Spatial patterns of bacterial signature biomarkers in marine sediments of the Gulf of Mexico. *Chem. Geol.* **238**, 168–179. (doi:10.1016/j.chemgeo.2006.11.007)
 87. Fang J, Shizuka A, Kato C, Schouten S. 2006 Microbial diversity of cold-seep sediments in Sagami Bay, Japan, as determined by 16S rRNA gene and lipid analyses. *FEMS Microbiol. Ecol.* **57**, 429–441. (doi:10.1111/j.1574-6941.2006.00126.x)
 88. Thurber AR, Levin LA, Rowden AA, Sommer S, Linke P, Kröger K. 2013 Microbes, macrofauna, and methane: a novel seep community fueled by aerobic methanotrophy. *Limnol. Oceanogr.* **58**, 1640–1656. (doi:10.4319/lo.2013.58.5.1640)
 89. Van Gaever S, Moodley L, Pasotti F, Houtekamer M, Middelburg JJ, Danovaro R, Vanreusel A. 2009 Trophic specialisation of metazoan meiofauna at the Håkon Mosby Mud Volcano: fatty acid biomarker isotope evidence. *Mar. Biol.* **156**, 1289–1296. (doi:10.1007/s00227-009-1170-9)
 90. Miyatake T, Moerdijk-Poortvliet TCW, Stal LJ, Boschker HTS. 2014 Tracing carbon flow from microphytobenthos to major bacterial groups in an intertidal marine sediment by using an in situ ¹³C pulse-chase method. *Limnol. Oceanogr.* **59**, 1275–1287. (doi:10.4319/lo.2014.59.4.1275)
 91. Cifuentes LA, Salata GG. 2001 Significance of carbon isotope discrimination between bulk carbon and extracted phospholipid fatty acids in selected terrestrial and marine environments. *Organ. Geochem.* **32**, 613–621. (doi:10.1016/S0146-6380(00)0198-4)
 92. Reeves EP *et al.* 2011 Geochemistry of hydrothermal fluids from the PACMANUS, Northeast Pual and Vienna Woods hydrothermal fields, Manus Basin, Papua New Guinea. *Geochim. Cosmochim. Acta* **75**, 1088–1123. (doi:10.1016/j.gca.2010.11.008)

93. Hensen C, Zabel M, Pfeifer K, Schwenk T, Kasten S, Riedinger N, Schulz HD, Boetius A. 2003 Control of sulfate pore-water profiles by sedimentary events and the significance of anaerobic oxidation of methane for the burial of sulfur in marine sediments. *Geochim Cosmochim. Acta* **67**, 2631–2647. (doi:10.1016/S0016-7037(03)00199-6)
94. Coffin R, Hamdam L, Plummer R, Smith J, Gardner J, Hagen R, Wood W. 2008 Analysis of methane and sulfate flux in methane-charged sediments from the Mississippi Canyon, Gulf of Mexico. *Mar. Petrol. Geol.* **25**, 977–987. (doi:10.1016/j.marpetgeo.2008.01.014)
95. Treude T, Niggemann J, Kallmeyer J, Wintersteller P, Schubert CJ, Boetius A, Jørgensen BB. 2005 Anaerobic oxidation of methane and sulfate reduction along the Chilean continental margin. *Geochim. Cosmochim. Acta* **69**, 2767–2779. (doi:10.1016/j.gca.2005.01.002)
96. Whiticar MJ. 1999 Carbon and Hydrogen isotope systematics of bacterial formation and oxidation of methane. *Chem. Geol.* **161**, 291–314. (doi:10.1016/S0009-2541(99)00092-3)
97. Joye SB, Boetius A, Orcutt BN, Montoya JP, Schulz HN, Erickson MJ, Lugo SK. 2004 The anaerobic oxidation of methane and sulfate reduction in sediments from Gulf of Mexico cold seeps. *Chem. Geol.* **205**, 219–238. (doi:10.1016/j.chemgeo.2003.12.019)
98. Kharlamenko VI, Kiyashko SI, Imbs AB, Vyshvartzev DI. 2001 Identification of food sources of invertebrates from the seagrass *Zostera marina* community using carbon and sulfur stable isotope ratio and fatty acid analyses. *Mar. Ecol. Progress Ser.* **220**, 103–117. (doi:10.3354/meps220103)
99. Lichtschlag A, Felden J, Brüchert V, Boetius A, de Beer D. 2010 Geochemical processes and chemosynthetic primary production in different thiotrophic mats of the Håkon Mosby Mud Volcano (Barents Sea). *Limnol. Oceanogr.* **55**, 931–949. (doi:10.4319/lo.2010.55.2.0931)
100. Deusner C, Holler T, Arnold GL, Bernasconi SM, Formolo MJ, Brunner B. 2014 Sulfur and oxygen isotope fractionation during sulfate reduction coupled to anaerobic oxidation of methane is dependent on methane concentration. *Earth Planet. Sci. Lett.* **399**, 61–73. (doi:10.1016/j.epsl.2014.04.047)
101. Magalhães VH *et al.* 2012 Formation processes of methane-derived authigenic carbonates from the Gulf of Cadiz. *Sedimentary Geol.* **243–244**, 155–168. (doi:10.1016/j.sedgeo.2011.10.013)
102. Van Lith Y, Warthmann R, Vasconcelos C, McKenzie JA. 2003 Sulphate-reducing bacteria induce low-temperature Ca-dolomite and high Mg-calcite formation. *Geobiology* **1**, 71–79. (doi:10.1046/j.1472-4669.2003.00003.x)
103. Mazzini A, Svensen H, Planke S, Forsberg CF, Tjelta TI. 2016 Pockmarks and methanogenic carbonates above the giant Troll gas field in the Norwegian North Sea. *Mar. Geol.* **373**, 26–38. (doi:10.1016/j.margeo.2015.12.012)
104. Stakes DS, Orange DL, PJD, Salamy KA, Maher N. 1999 Cold-seeps and authigenic carbonate formation in Monterey Bay, California. *Mar. Ecol.* **159**, 93–109. (doi:10.1016/S0025-3227(98)00200-X)
105. Suess E, Balzer W, Hesse K-F, Müller PJ, Ungerer CA, Wefer G. 1982 Calcium carbonate hexahydrate from organic-rich sediments of the Antarctic shelf: precursors of glendonites. *Science* **216**, 1128–1130. (doi:10.1126/science.216.4550.1128)
106. Vasconcelos C, McKenzie JA, Bernasconi SM, Grujic D, Tien AJ. 1995 Microbial mediation as a possible mechanism for natural dolomite formation at low temperatures. *Nature* **377**, 220–222. (doi:10.1038/377220a0)
107. Greinert J, Bollwerk SM, Derkachev A, Bohrmann G, Suess E. 2002 Massive barite deposits and carbonate mineralization in the Derugin Basin, Sea of Okhotsk: precipitation processes at cold seep sites. *Earth Planet. Sci. Lett.* **203**, 165–180. (doi:10.1016/S0012-821X(02)00830-0)
108. Feng D, Roberts HH. 2010 Initial results of comparing cold-seep carbonates from mussel- and tubeworm-associated environments at Atwater Valley lease block 340, northern Gulf of Mexico. *Deep Sea Res. II Top. Stud. Oceanogr.* **57**, 2030–2039. (doi:10.1016/j.dsr2.2010.05.004)
109. Glover EA, Taylor JD. 2010 Needles and pins: acicular crystalline periostracal calcification in venerid bivalves (Bivalvia: Veneridae). *J. Molluscan Stud.* **76**, 157–179. (doi:10.1093/mollus/eyp054)
110. Taylor JD, Glover EA, Peharda M, Bigatti G, Ball AD. 2004 Extraordinary flexible shell sculpture: the structure and formation of calcified periostracal lamellae in *Lucina pensylvanica* (Bivalvia: Lucinidae). *Malacologia* **46**, 277–294.
111. Gillan DC, De Ridder C. 2004 Iron encrustation of the bivalve *Montacuta ferruginosa*. *J. Mar. Biol. Assoc. UK* **84**, 1213–1214. (doi:10.1017/S0025315404010677h)
112. Gillan DC, De Ridder C. 2001 Accumulation of a ferric mineral in the biofilm of *Montacuta ferruginosa* (Mollusca, Bivalvia): biomineralization, bioaccumulation, and inference of paleoenvironments. *Chem. Geol.* **177**, 371–379. (doi:10.1016/S0009-2541(00)00420-4)
113. Gillan DC, Speksnijder AGCL, Zwart G, De Ridder C. 1998 Genetic diversity of the biofilm covering *Montacuta ferruginosa* (Mollusca, Bivalvia) as evaluated by denaturing gradient gel electrophoresis analysis and cloning of PCR-amplified gene fragments coding for 16S rRNA. *Appl. Environ. Microbiol.* **64**, 3464–3472.